# Unraveling the Role of 12-*cis*-Oxo-Phytodienoic Acid in the Wound Response of *Arabidopsis thaliana*: Insights from Transcriptomic and Complementation Studies

**Khansa Mekkaoui[1], Ranjit Baral[1], Fiona Smith[1], Moritz Klein[2], Ivo Feussner[2], Bettina Hause[1,*]**

[1] Department of Cell and Metabolic Biology, Leibniz Institute of Plant Biochemistry, Weinberg 3, D-06120 Halle/Saale, Germany

[2] Department of Plant Biochemistry, Albrecht-von-Haller-Institute for Plant Sciences and Goettingen Center for Molecular Biosciences (GZMB), University of Goettingen, Justus-von-Liebig-Weg 11, 37077 Göttingen, Germany

Corresponding author: Bettina Hause, Bettina.Hause@ipb-halle.de

**Running title:**

Signaling and compartmentalization of OPDA

**Abstract**

In addition to jasmonoyl-isoleucine (JA-Ile), a well-established signaling molecule for plant growth and defense, its precursor, *cis*-12-oxo-phytodienoic acid (OPDA), is thought to possess independent signaling functions. Its perception in vascular plants is still uncharacterized. Several OPDA functions in Arabidopsis were inferred from a mutant that is affected in the function of the OPDA REDUCTASE3 (OPR3), catalyzing the conversion of OPDA within peroxisomes. Recently, *opr3* plants were found to accumulate JA-Ile via a cytosolic OPR2-mediated bypass. Given the uncoupling of OPDA and JA biosynthesis in the JA-deficient mutant *opr2opr3*, potential OPDA signaling was investigated by a transcriptome approach comparing wild type, *opr2opr3* and the JA- and OPDA-deficient mutant *allene oxide synthase*. Dissecting the wound response of seedlings revealed that OPDA lacked a transcriptional signature, and that previously characterized OPDA-response genes were wound-induced independently of OPDA. Exogenous application of OPDA to *opr2opr3* seedlings led to JA-Ile formation and signaling even in absence of OPR2 and OPR3 and resulted in activation of sulfur assimilation. These divergent responses to endogenously synthesized and applied OPDA suggest a compartmentalization of endogenous OPDA which was investigated by a trans-organellar complementation approach. OPR3 complemented the *opr2opr3* mutant in terms of fertility and wound-induced JA-Ile production irrespective of its subcellular localization. *In vitro* enzymatic activity of OPR3, however, showed conversion of OPDA and 4,5-didehydro-JA (4,5-ddh-JA), therefore not allowing to conclude which compound is translocated. Dissecting the conversion of either OPDA or 4,5-ddh-JA by OPR2 and OPR1 organelle variants pointed to a strong OPDA compartmentalization supporting its lacking signaling capacity.

## Introduction

Jasmonic acid (JA) and its bioactive form jasmonoyl-isoleucine (JA-Ile) function primarily as signaling molecules coordinating plant growth and reproduction and responses to biotic and abiotic stresses (Li et al., 2022; Wang et al., 2019; Wasternack and Hause, 2013; Zhang et al., 2023). They play a central role in the defense of plants to mechanical damage and herbivory, as JA-Ile rapidly accumulates at the site of injury and acts as a signaling molecule by triggering a cascade of defense responses (Koo and Howe, 2009; Wasternack, 2019). JA-Ile signaling involves a series of molecular events mediated by its perception by the F-box protein CORONATINE INSENSITIVE 1 (COI1) leading to the degradation of the JASMONATE ZIM-DOMAIN (JAZ) repressors, hence the release of the expression of JA-responsive genes (Chini et al., 2007; Monte et al., 2022; Sheard et al., 2010; Thines et al., 2007; Xie et al., 1998; Xu et al., 2002; Yan et al., 2018).

One major intermediate in the formation of the bioactive JA-Ile, *cis*-12-oxo-phytodienoic acid (OPDA), has been known to be also a signaling molecule with independent functions from JA-Ile (Dave and Graham, 2012; Jimenez-Aleman et al., 2022; Liu and Park, 2021; Wasternack and Strnad, 2016). OPDA formation takes place in the chloroplast via the octadecanoid pathway, by oxygenation of α-linolenic acid by 13-lipoxygenases (LOXs) and the coupled actions of ALLENE OXIDE SYNTHASE (AOS) and ALLENE OXIDE CYCLASE (AOC) (Andreou and Feussner, 2009; Bannenberg et al., 2009; Feussner and Wasternack, 2002) (Figure 1A). Metabolization of OPDA into JA occurs after its transfer to peroxisomes, where the reduction of its cyclopentenone ring by OPDA REDUCTASE3 (OPR3) and three rounds of β-oxidation take place (Schaller and Stintzi, 2009; Schaller et al., 2000; Wasternack and Hause, 2013). A parallel hexadecanoid pathway gives rise to *dinor*-12-oxo-phytodienoic acid (*dn*-OPDA), which in turn is converted to JA following the same pathway as OPDA, but with two rounds of β-oxidation only (Weber et al., 1997).

The putative distinct function of OPDA in Angiosperms partially derives from its function in lower plants by inducing defense- and growth inhibition-related transcriptional reprogramming in *Marchantia polymorpha* (Chini et al., 2023; Monte *et al.*, 2022; Monte et al., 2018; Monte et al., 2020). Such JA-independent functions of OPDA were also characterized in higher plants for different vegetative processes including initiation of tendril coiling in *Bryonia dioica* (Stelmach et al., 1998), regulation of embryo development in *Solanum lycopersicum* (Goetz et al., 2012), and inhibition of seed germination and induction of stomatal closure in *Arabidopsis thaliana* (Chang et al., 2023; Dave et al., 2011; Savchenko and Dehesh, 2014). Despite its perception being not

identified in Arabidopsis, OPDA was shown to act as signaling molecule by transcriptionally inducing a set of genes, which is not induced by JA (Taki et al., 2005). These OPDA-specific response genes were characterized as wound- and OPDA-responsive in a COI1-independent manner and encompassed mainly stress-responsive genes, e.g. *DRE-BINDING PROTEIN 2A* (*DREB2A)*, *FAD-LINKED OXIDOREDUCTASE* (*FAD-OXR), SALT TOLERANCE ZINC FINGER* (*ZAT10)* and the glutaredoxin member *GRX480*. OPDA contains an α, β-unsaturated carbonyl group which is thought to react with nucleophilic molecules by Michael addition (Alméras et al., 2003). The electrophilic nature of oxylipins could convey biological activities, as deduced from the accumulation of oxylipins adducts, including OPDA-GSH conjugates, during the hypersensitive response in pathogen-elicited tobacco leaves (Davoine *et al.*, 2006). OPDA binding to the CYCLOPHILIN20-3 (CYP20-3) was suggested to trigger the formation of the cysteine synthase complex activating sulfur assimilation to regulate cell redox homeostasis through mediation of *TGACG-BINDING* (TGA) transcription factors (Müller et al., 2017; Park et al., 2013). Here, CYP20-3-dependent OPDA signaling induces high levels of GSH leading to a retrograde signaling, which coordinates expression of OPDA-induced genes (Adhikari and Park, 2023). These transcriptional changes in Arabidopsis induced by OPDA through CYP20-3 module and/or additional uncharacterized mechanism consolidated the hypothesis of its function not limited to being only a JA precursor (Liu and Park, 2021).

The previous work characterizing OPDA signaling and JA-independent functions in Arabidopsis relied mainly on the use of the *opr3* mutant as the genetic background where OPDA and JA biosynthesis were uncoupled due to missing OPR3 (Stintzi and Browse, 2000; Stintzi et al., 2001). The *opr3* mutant is male sterile like the *aos* mutant being deficient in OPDA and JA (Browse, 2009; Stintzi and Browse, 2000; von Malek et al., 2002). Both mutants show defects in anther dehiscence, stamen elongation and pollen development showing that these defects were due to impairments in JA production. Persistent resistance of the *opr3* mutant against necrotrophic pathogens initially hinted towards a defense function of OPDA, but further studies uncovered an OPR3-independent pathway leading to JA/JA-Ile formation through the cytosolic OPR2 in the *opr3* mutant (Chini et al., 2018). Low JA-Ile formation in the *opr3* mutant rather than OPDA was shown to be responsible of its resistance, hence challenging the suggested JA-independent OPDA signaling function (Chini et al., 2018). Thus, the recently identified "leakiness" of the *opr3* mutant and formation of JA-Ile via bypassing the OPR3 (Figure 1A) questioned previously identified

108 functions of OPDA. Consequently, OPDA-specific signaling exclusively analyzed with the *opr3*
109 mutants requires further studies.
110 This study re-addressed the question whether OPDA can function as an independent
111 signaling molecule in Arabidopsis besides being a JA precursor. Using the *opr2opr3* mutant where
112 formation of JA/JA-Ile does not occur (Chini et al., 2018), we investigated the effects of basal and
113 wound-induced OPDA on gene expression in seedlings of *A. thaliana*. The results suggested that
114 the endogenously formed OPDA is unlikely to be responsible to mediate gene expression, while
115 exogenous supply of OPDA resulted in a distinct signaling. Exogenously supplied OPDA is
116 predominantly detoxified and partially converted to JA/JA-Ile, hinting towards a
117 compartmentalization of the endogenously formed OPDA. Therefore, we addressed the question
118 of the occurrence of OPDA within the cell and whether it could be perceived. A trans-organellar
119 complementation approach showed that OPDA is likely to be confined to the cell compartments
120 where it is synthesized and metabolized. Instead, 4,5-ddh-JA appears to be the mobile compound
121 within the plant cell supporting the assumption that OPDA has no signaling function in wounded
122 seedlings.
123
124
125 **Results**
126 **A JA positive feedback loop during development is responsible for the tissue capability to**
127 **produce OPDA.**
128 The *opr2opr3* double mutant was characterized as JA-deficient, with JA formation through the
129 peroxisomal OPR3 and alternatively through the cytosolic OPR2 being both interrupted (Chini et
130 al., 2018). JA deficiency is associated with a decrease in the accumulation of JA-biosynthesis
131 enzymes, among them specifically the AOC, due to the disruption of the JA positive feedback loop
132 during development (Stenzel et al., 2003). Indeed, *opr2opr3* and the *aos* accumulated statistically
133 lower levels of the AOC proteins in their seedlings in comparison to wild-type (Col-0) seedlings
134 (Supplemental Figure 1A, B). These diminished AOC protein levels correlated with lower
135 background and wound-induced levels of OPDA in the *opr2opr3* mutant compared to the wild
136 type, whereas the JA levels remained at the detection limit (around 0.002 nmol/g of fresh weight)
137 in the mutants (Supplemental Figure 1C, D), which contrast to *opr3* mutant plants accumulating
138 JA levels after wounding of around 0.2 nmol/g of fresh weight (Stintzi et al., 2001). This confirmed
139 the stronger JA deficiency of *opr2opr3* compared to the *opr3* mutant.

140 Due to the partial OPDA deficiency of *opr2opr3* seedlings, it was crucial to normalize the
141 levels with those of the wild type prior to investigating OPDA signaling within this mutant. To
142 achieve this, we mimicked the missing JA positive feedback loop in the *opr2opr3* and *aos* mutants
143 by supplying seedlings with 1 µM JA methyl ester (MeJA) during development to increase the
144 AOC protein levels (Supplemental Figure 2A). In contrast to water (mock-)pretreated seedlings,
145 seedlings pretreated with MeJA during development exhibited increased AOC protein levels in
146 wild type and both mutants (Figure 1B). Notably, this increase was more pronounced in the mutants
147 resulting in AOC protein levels in *opr2op3* and *aos* seedlings matching those of wild type seedlings
148 (Figure 1C). Transcript accumulation of the JA biosynthesis enzymes *LOX2*, *AOS*, *AOC2* and
149 *OPR3* determined by RT-qPCR corroborated the function of the JA positive feedback loop: MeJA
150 pretreatment during development resulted in a compensation of their basal transcript levels in the
151 mutants compared to wild type (Figure 1D). They all are, however, highly induced upon wounding
152 in wild-type seedlings, but their induction is significantly lower in the mutants (Figure 1D). This
153 shows that the MeJA pretreatment did not lead to a wound-induced JA-Ile signaling in the JA-
154 deficient mutants. Most importantly, however, the restoration of AOC protein content in the
155 *opr2op3* enhanced its basal and wound-induced OPDA and *dn*-OPDA levels to the levels of wild
156 type but did not affect the OPDA deficiency of the *aos* mutant (Figure 1E). Despite the
157 accumulation of low residual levels of JA in *opr2opr3* and *aos* seedlings upon pretreatment, wound
158 induction of JA and JA-Ile was only observed in the wild-type seedlings. This validates the JA
159 deficiency of both mutant lines and the exclusive OPDA enhancing role of the developmental JA-
160 feedback loop for the *opr2opr3* mutant (Figure 1E).
161
162 **A comparative transcriptomics approach shows a JA-specific but not an OPDA-specific**
163 **response to wounding.**
164 OPDA signaling in Arabidopsis was previously inferred from its capacity to mediate transcriptional
165 changes by inducing a specific set of OPDA-responsive genes in the "leaky" *opr3* single mutant
166 (Ribot et al., 2008; Taki et al., 2005). Another putative OPDA-signaling pathway was based on the
167 detected binding of OPDA to CYP20-3, which in turn transcriptionally induces TGA transcription
168 factors (Park et al., 2013). To further clarify this signaling function, a comparative transcriptomics
169 approach was set between wild-type and *opr2opr3* seedlings. To uncouple putative OPDA
170 signaling from wound-induced signaling processes, *aos* seedlings were included as a negative
171 control, since both JA and OPDA production are abolished in this mutant (Supplemental Figure

172 2B). mRNA sequencing of MeJA-pretreated seedlings from Col-0, *opr2opr3* and *aos* was
173 performed using unwounded seedlings (control) and seedlings harvested 1 h after wounding. The
174 overall wound-induced response showed a significant transcriptional change in all three genotypes
175 (Supplemental Figure 3). Here, a strong similarity between the transcriptomes of *opr2opr3* and *aos*
176 seedlings was evident in the expression heatmap and principal component analysis (PCA)
177 irrespective of the condition (Supplemental Figure 3). Indeed, the highest number of differentially
178 expressed genes (DEGs) was common to all three genotypes and were enriched in genes involved
179 in stress, oxygen, and abiotic stimulus responses (Figure 2A, B). This general stress response was
180 therefore rather wound-inducible but independent from the JA pathway. Interestingly, this group
181 contained known stress-responsive genes with several genes being previously reported as OPDA-
182 responsive, such as *DREB2A*, *FAD-OXR, ZAT10* and *GRX480* (Taki et al., 2005) (Figure 2C, D).
183 Their wound-responsive induction in *aos* seedlings indicated that they are more likely to be
184 associated with a JA-independent wound-induced stress response than with an OPDA-mediated
185 response.
186 In wild-type seedlings, the signaling mediated by JA/JA-Ile was obvious as it shaped
187 differentially the transcriptome already by sustaining statistically differential basal levels of 58 JA-
188 responsive genes in comparison to the mutants (Supplemental Figure 4A, B). Wounding of wild-
189 type seedlings resulted in a transcriptional change enriched in genes related to JA and immune
190 responses (Supplemental Figure 4C). These transcriptional responses, notably of genes encoding
191 JAZ transcription factors and other JA-responsive genes, such as *CHLOROPHYLLASE 1* (*CLH1)*
192 and *N-ACETYLTRANSFERASE ACTIVITY 1* (*NATA1)*, were dampened in the *opr2opr3* and *aos*
193 mutants confirming the JA dependence of their induction upon wounding (Supplemental Figure
194 4D). These data suggest that next to a common wound response, JA/JA-Ile are main mediators of
195 wound-induced transcriptional changes in wild-type seedlings.
196
197 **Wound-induced and exogenously applied OPDA resulted in different alterations of the**
198 **transcriptome in *opr2opr3* seedlings.**
199 To identify OPDA-regulated genes, transcriptional differences between *opr2opr3* and *aos* were
200 dissected and indicated a restricted number of DEGs at control and wounding conditions (Figure
201 3A). Except for the mutated genes, which showed diminished expression in the respective mutant
202 backgrounds (*AOS*, *OPR2*, and *OPR3*), only nine specific genes exhibited differential expression
203 in *opr2opr3* seedlings compared to *aos* seedlings, regardless of the experimental condition (Figure

204 3B, C). These genes encode five RNA species and four proteins, among them one cyclic nucleotide-
205 gated ion channel (*CNGC11*), one cytochrome P450 (*CYP81D11*), and two hypothetical proteins.
206 This is a very narrow or almost no difference between transcriptomic profiles of the mutants,
207 although there were significantly enhanced OPDA levels in the *opr2opr3* mutant compared to *aos*
208 (Figure 1E). These results make an OPDA-mediated gene expression in wounded seedlings of the
209 *opr2opr3* mutant unlikely.

210 Previous work demonstrated a signaling role of OPDA in Arabidopsis by its exogenous
211 supply to wild-type plants or to the *opr3* mutant (Park et al., 2013; Ribot et al., 2008; Taki et al.,
212 2005). To determine whether the origin of OPDA caused the different outcomes, RNAseq data
213 resulting from wounding of *opr2opr3* seedlings (= endogenous rise of OPDA) were compared to
214 transcriptomic data generated from *opr2opr3* seedlings, which were treated with 25 µM OPDA for
215 30 min (= exogenous supply of OPDA). OPDA treatment resulted in transcriptional changes that
216 were highly different from those induced by wounding (Supplemental Figure 5). The clustering of
217 DEGs induced by OPDA treatment in comparison to DEGs induced by wounding showed an
218 exclusive induction of JA signaling and sulfate reduction by OPDA application (Supplemental
219 Figure 5). To get a deeper insight into this JA-mediated response occurring in *opr2opr3* seedlings
220 upon OPDA treatment, expression levels of JA responsive genes were determined in comparison
221 to wounded seedlings from wild type and both mutants (Figure 4). OPDA-treated *opr2opr3* and
222 wounded wild-type seedlings shared the up-regulation of several JA marker genes, such as those
223 encoding JAZ transcription factors and JA biosynthesis enzymes (Figure 4A). Validation of
224 transcript accumulation of *JAZ2*, *JAZ7*, *JAZ13* and *CHL1* by RT-qPCR confirmed their exclusive
225 induction in *opr2opr3* seedlings upon OPDA application but not upon endogenous OPDA
226 accumulation by wounding (Figure 4B). This hints towards the conversion of the exogenously
227 applied but not the endogenously formed OPDA to JA/JA-Ile despite the loss of OPR3 and OPR2
228 in the *opr2opr3* background. OPDA and JA levels in *opr2opr3* seedlings determined after
229 wounding and OPDA treatment showed unequivocally that *opr2opr3* seedlings accumulated
230 significantly higher levels of JA-Ile following OPDA application in comparison to wounding
231 (Figure 4C). Despite these levels being lower than the wild-type JA-Ile levels, they correlated with
232 the activated JA signaling in *opr2opr3* seedlings after OPDA application. Interestingly, the OPDA-
233 fed *opr2opr3* seedlings accumulated only slightly higher OPDA levels than the wounded seedlings,
234 whereas *dn*-OPDA accumulated significantly only following endogenous OPDA formation after
235 wounding (Figure 4C). This suggests that the exogenously applied OPDA did not engage in β-

236 oxidation to form *dn*-OPDA in the *opr2opr3* mutant unlike the endogenously formed OPDA, which
237 is able to enter the β-oxidation cycle leading to *dn*-OPDA accumulation (Chini et al., 2018).
238 Nevertheless, JA-Ile formation after OPDA application without accumulation of *dn*-OPDA hints
239 towards its conversion to 3-oxo-2-(20(Z)-pentenyl)-cyclopentane-1-octanoic (OPC-8:0) (Figure
240 1A) in the cytosol and its further metabolization into JA through β-oxidation in the peroxisome.
241 Here, the third OPR isoenzyme, OPR1, which is cytosolic and has some activity towards OPDA
242 (Chini et al., 2018), might contribute to the conversion of OPDA.

243 OPDA application to the *opr2opr3* mutant showed a significant induction of a second sub-
244 cluster of genes belonging to sulfate reduction and assimilation pathway as well as the
245 phosphorelay signal transduction pathway (Figure 4A, Supplemental Figure 5). These genes were
246 not induced by the endogenous rise of OPDA and included genes encoding sulfate reductases, such
247 as APS REDUCTASE1 (APR1), APR2 and APR3, ATP-SULFURYLASE1 (APS1), and
248 SULFATE-DEFICIENCY INDUCED (SDI1) (Figure 4D). This is in line with the previously
249 reported induction of sulfur metabolism by OPDA binding to the CYP20-3 module (Park et al.,
250 2013). These results raise the question whether this is due to a mis-localization of the exogenously
251 provided compound, whereas OPDA synthesized following wounding is compartmentalized and
252 therefore does not induce the responses that the exogenously supplied OPDA does.
253

254 **Test for subcellular distribution of the endogenously produced OPDA using a trans-**
255 **organellar complementation of the *opr2opr3* mutant.**

256 The data obtained from wounded seedlings of *opr2opr3* and described above suggest that
257 endogenously produced OPDA does not exhibit signaling capacity. This leads to the question,
258 whether OPDA is restricted to the cell compartments of its synthesis, transfer and metabolization,
259 namely plastids, cytosol and peroxisomes, respectively. To test its putative translocation to other
260 cell compartments, a trans-organellar complementation approach according to (Mehrshahi et al.,
261 2013) using the *opr2opr3* mutant was performed. OPR3 was targeted to different organelles in the
262 *opr2opr3* mutant, and the fertility of these plants was checked. A rescue of the JA-deficiency
263 phenotype of the *opr2opr3* mutant would indicate whether its substrate, OPDA, is able to
264 translocate to the tested organelles (Supplemental Figure 6).

265 OPR3 is a peroxisome-localized protein and is imported into the matrix of peroxisomes
266 through the peroxisomal targeting signal type 1 (PTS1) consisting of a tripeptide at the extreme
267 carboxy-tail of the protein (Gould et al., 1989). OPR3 contains a C-terminal SRL which is a

268 variation of the prototypic PTS1 signal SKL. The removal of the SRL signal resulted in a cytosolic
269 localization of a fusion of OPR3ΔSRL with YFP when transiently expressed in *Nicotiana*
270 *benthamiana* leaves indicating that import into peroxisomes was abolished (Supplemental Figure
271 7A, B). Targeting of OPR3 to the nucleus, cytosol, plastids, mitochondria, and endoplasmic
272 reticulum (ER) was done by fusing OPR3ΔSRL with the respective targeting signals or target
273 peptides (Supplemental Table 1). Validation of the subcellular localization of the different
274 organelle variants of OPR3 with co-localization studies in *N. benthamiana* protoplasts was
275 performed using established organelle markers (Stellmach et al., 2022) and indicated correct
276 subcellular localizations of OPR3 compared to the markers independently of the position of the
277 YFP fluorescent tag (Supplemental Figure 8). Stable transgenic *opr2opr3* lines complemented with
278 the organelle variants of OPR3ΔSRL fused to YFP were generated and resulted in clear subcellular
279 localizations of OPR3-YFP to the nucleus, cytosol, chloroplast stroma, mitochondria, and ER
280 (Supplemental Figure 7C-G).

281 The main phenotypic feature of JA-deficient and JA-insensitive Arabidopsis mutants is the
282 male sterility, which is also characteristic for *opr2opr3* plants and is visible by defects in filament
283 elongation, pollen release and seed set (Browse, 2009). Plants of *opr2opr3* transformed with an
284 empty vector (EV) showed short stamens with non-dehiscing anthers (Figure 5A, B), similar to the
285 reported male sterility phenotype of the *opr3* mutant (Stintzi and Browse, 2000). As a positive
286 control, the complementation of *opr2opr3* with the peroxisome targeted OPR3 showed full rescue
287 of the flower phenotype (Figure 5C). Interestingly, all other tested organelle-variants of OPR3 also
288 rescued the flower sterility and showed open flowers like the wild type with elongated stamens and
289 anthers releasing pollen (Figure 5D-H). This rescue of sterility translated also in the ability of the
290 lines to form siliques containing seeds. The only exception were plants complemented with the
291 ER-targeted OPR3 having partial rescue of flower fertility only. These plants formed fewer and
292 smaller siliques compared to the wild type (Figure 5F). It is tempting to speculate that OPR3
293 localized to the ER might have access only to limited amounts of its substrate, leading to partial
294 JA/JA-Ile biosynthesis only.

295 Reconstitution of the JA pathway in vegetative tissue of the *opr2opr3* complementation
296 lines was analyzed by determination of wound-induced levels of OPDA, JA and JA-Ile in two-
297 week-old seedlings. Hormone levels of *opr2opr3* complemented with OPR3 targeted to either
298 peroxisomes, cytosol or mitochondria were compared to those of wild type and *opr2opr3*
299 transformed with an empty vector. Data from two independent transformed lines each revealed that

300 complementation of *opr2opr3* with OPR3 restored the JA/JA-Ile levels to wild-type levels (Figure
301 5I). These results show the reconstitution of JA biosynthesis by OPR3 localized to all the tested
302 compartments.
303
304 **Trans-organellar complementation with OPR2 and OPR1 to determine whether OPDA or 4,**
305 **5-ddh-JA is the translocating substrate.**
306 JA biosynthesis in *opr2opr3* complemented with OPR3 located in different organelles would occur
307 only if its substrate, OPDA, is able to translocate to these compartments. However, as an alternative
308 pathway, OPDA could enter directly the β-oxidation as reported recently (Chini et al., 2018). This
309 would result in formation of 4,5-ddh-JA, which might be metabolized by OPR3 irrespective of the
310 organellar location. Conversion of 4,5-ddh-JA to JA by OPR3 was tested by *in vitro* enzymatic
311 assay and showed that OPR3 reduces 4,5-ddh-JA *in vitro*, however to a lesser extent than OPDA
312 (Supplemental Figure 9). Based on substrate consumption after 10 min, only half of the given 4,5-
313 ddh-JA was reduced while OPDA was completely converted to OPC-8. The control reactions with
314 inactivated enzyme showed no reduction activity. The results clearly show that OPR3 is able to
315 reduce both cyclopentenones, 4,5-ddh-JA and OPDA, *in vitro*. In addition, it has been shown by
316 recombinant enzymatic assays that OPR2 but not OPR1 is able to reduce 4,5-ddh-JA (Chini et al.,
317 2018). Conversely, OPR1 is able to reduce OPDA although with very low efficiency but OPR2 is
318 not (Schaller et al., 2000). To determine whether OPDA or 4,5-ddh-JA is the substrate able to
319 translocate to the tested cell compartments and specifically to cell compartments unrelated to the
320 location of JA biosynthesis, peroxisomal, cytosolic and mitochondrial variants of OPR1 and OPR2,
321 both fused to YFP, were used to complement the *opr2opr3* mutant. Both OPRs localized to the
322 cytosol, whereas addition of a C-terminal SKL and an N-terminal mitochondrial target sequence
323 led to localization in peroxisomes and mitochondria, respectively (Figure 6A). All three variants
324 expressing OPR2 rescued the flower sterility and showed open flowers like the wild type with
325 elongated stamens and anthers releasing pollen (Figure 6B) as well as formation of seed-containing,
326 fully developed siliques (Figure 6C). In contrast, expression of OPR1 located to peroxisomes was
327 the only OPR1 variant leading to a rescue of the flower sterility, whereas targeting OPR1 to the
328 cytosol led to partial rescue of flower fertility only and targeting OPR1 into the mitochondria did
329 not restore the fertility (Figure 6B, C). These data were supported by the fact that only seedlings
330 harboring the OPR2 variants and peroxisomal-located OPR1 were able to accumulate JA and JA-
331 Ile upon wounding (Figure 6D), although all lines accumulated similar levels of OPDA

332 (Supplemental Figure 10). The JA/JA-Ile levels were lower than those of wounded wild-type
333 seedlings, but the significantly increased levels in comparison to *opr2opr3* showed the capability
334 of these plants to produce JA/JA-Ile. Most importantly, however, expression of OPR1 located to
335 mitochondria did not restore fertility nor JA/JA-Ile levels. Since OPR1 does not convert 4,5-ddh-
336 JA to JA, this result points to the fact that 4,5-ddh-JA but not OPDA might be the compound to be
337 converted by OPR2 or OPR3 in different organelles.
338
339
340 **Discussion**
341 JA plays a major role in growth and defense against pathogens, herbivory attacks and mechanical
342 wounding. Its signaling through the bioactive JA-Ile is well established in Angiosperms, while in
343 lower plants, such as *M. polymorpha*, OPDA and its β-oxidation product *dn*-OPDA are bioactive
344 (Chini et al., 2023; Monte et al., 2022; Monte et al., 2018; Monte et al., 2020). Given that *A.*
345 *thaliana* plants produce both compounds, possible function of OPDA as a signaling molecule
346 independently from JA was proposed. OPDA was shown to induce a distinct transcriptional change
347 from JA when exogenously applied to Arabidopsis plants (Ribot et al., 2008; Taki et al., 2005).
348 Additionally, OPDA´s involvement in processes like seed germination and stomatal closure was
349 demonstrated (Chang et al., 2023; Dave et al., 2011; Savchenko and Dehesh, 2014). The
350 mechanism by which OPDA exerts these functions in vascular plants is, however, still elusive
351 (Jimenez-Aleman et al., 2022). A major genetic background used for studying OPDA functions
352 was the *opr3* mutant (Browse, 2009). Recently, an OPR3-independent pathway of JA formation
353 through the cytosolic isoenzyme OPR2 has been identified (Chini et al., 2018). Hence, uncoupling
354 of JA production from OPDA was not achieved in this mutant, and the characterized functions of
355 OPDA cannot be attributed to OPDA with certainty. Here, we addressed the question of whether
356 OPDA functions independently from JA as a signaling molecule in Arabidopsis, by utilizing the
357 *opr2opr3* mutant, which is more JA-deficient than *opr3* (Chini et al., 2018).
358 The use of the *opr2opr3* mutant is limited by its lower production of OPDA in comparison
359 to the wild type due to the disrupted JA positive feedback loop as indicated by reduced protein
360 levels of the biosynthesis enzymes, such as AOC (Wasternack and Hause, 2013). The enhancement
361 of the AOC levels and subsequent OPDA production in the JA-deficient mutants was achieved by
362 restituting the JA feedback loop through a repetitive supply of MeJA to seedlings during
363 development (Figure 1). This result validated the role of the JA positive feedback loop in the

regulation of the basal levels of the biosynthetic enzymes and setting the tissue ability to produce OPDA and putatively JA (Stenzel et al., 2003).

**The wounding response of wild-type seedlings involves JA-dependent and independent processes.**

To inspect the separate roles of OPDA and JA upon wounding, a comparative analysis of the transcriptomes of seedlings of wild type, *opr2opr3* and *aos* was carried out. The transcriptomic change induced by wounding in wild-type seedlings involved an up-regulation of genes previously identified as JA-dependent or associated with immune responses, validating the specific signaling role of JA-Ile in the wound response of seedlings as it has been described for mature leaves of Arabidopsis and other plant species (Chung et al., 2008; Howe, 2004; Koo and Howe, 2009; Wasternack, 2006). Unexpectedly, seedlings of the *aos* mutant being deficient in synthesis of JA and OPDA, also showed a major transcriptional change upon wounding that was common to the *opr2opr3* mutant and the wild type (Figure 2). The transcriptional response was significantly enriched in general stress response pathways, with an induction of oxidative stress- and transcription-related genes. This implies that JA-independent signaling processes occur in response to mechanical wounding leading to transcriptional reprogramming. Among such processes, water stress might contribute to the regulation of wound-responsive genes in a JA-independent manner (Reymond et al., 2000). Ethylene and abscisic acid (ABA) also contribute to the wound response by regulating photosynthesis and drought responsive genes, respectively (Delessert et al., 2004). An ABA-dependent and JA-independent transcriptional regulation of wax biosynthesis to seal the wounded sites of Arabidopsis leaves has been recently characterized, but appears to be controlled post-translationally by JA (Lewandowska et al., 2023). As plants defective in JA/JA-Ile biosynthesis or perception are severely diminished in their defense response (Browse, 2009; Goodspeed et al., 2012; Guo et al., 2018; Verhage et al., 2011), the JA-independent wound response has rather limited contribution to plant defense and might only mitigate the adverse effects of wounding itself.

**An OPDA-specific transcriptional response is missing in wounded *opr2opr3* seedlings, but specific pathways are activated by the exogenous application of OPDA.**

The general stress response that was both JA and OPDA-independent, comprised genes that were previously identified as OPDA-specific response genes, such as *FAD-OXR*, *DREB2A*, *ZAT10* and

396 *GRX480* (Taki et al., 2005). These genes did not show differential expression when the
397 transcriptomes of *opr2opr3* and *aos* were compared. Given that they were equally induced in
398 seedlings of *opr2op3* and *aos* mutants, their induction by wounding is OPDA-independent (Figure
399 2). Several abiotic stresses were reported to up-regulate the same genes (Davletova et al., 2005;
400 Mittler et al., 2006; Mizoi et al., 2019; Sakuma et al., 2006), further indicating their independence
401 from OPDA. Moreover, direct comparison of transcriptomes from wounded *opr2opr3* and *aos*
402 seedlings with standard cut-off parameters did not yield a significant list of putative OPDA-
403 regulated genes further confirming the absence of an OPDA signaling (Figure 3). This could be
404 due to three facts: (i) A putative receptor for OPDA might be missing in *A. thaliana*, (ii) OPDA
405 remains sequestered in the plastids by its biosynthetic enzymes (Pollmann et al., 2019), and (iii)
406 OPDA is converted to 4,5-ddh-JA, which does not have signaling capacity (Chini et al., 2018).
407 Regarding perception of OPDA, evolutionary studies of the JA-Ile co-receptor COI1 showed that
408 the Arabidopsis protein does not perceive OPDA or *dn*-OPDA, dismissing possible signaling of
409 OPDA through COI1 in this plant (Monte et al., 2022). Moreover, it has been shown that *dn-iso*-
410 OPDA rather than *dn*-OPDA is the bioactive molecule in mosses, and that this compound does not
411 occur in *A. thaliana* (Chini et al., 2023). The transcriptomic data obtained from *opr2opr3* and *aos*
412 therefore point to the fact that OPDA or its homolog *dn*-OPDA are not perceived by COI1 or any
413 other receptor in Arabidopsis.

414 The transcriptional signature of OPDA was predominantly observed in experiments relying
415 on its exogenous application (Park et al., 2013; Ribot et al., 2008; Taki et al., 2005). Therefore, we
416 compared the transcriptional changes following application of OPDA to *opr2opr3* seedlings with
417 those by wound-induced, endogenously produced OPDA. This comparison revealed an up-
418 regulation of JA-Ile signaling components only by the exogenous supply with OPDA and
419 correlated with a significant accumulation of JA-Ile (Figure 4). Beside not uncoupling JA-Ile
420 biosynthesis from OPDA, this approach indicates that JA-Ile formation in the *opr2opr3*
421 background could occur through OPR1 due to the reported low activity of OPR1 towards *cis*-
422 OPDA (Schaller et al., 2000). In this case, exogenously supplied OPDA might flood the cytosol
423 and therefore is available to the cytosolic OPR1, whereas the endogenously produced OPDA might
424 either stay in the plastid stroma (Pollmann et al., 2019) or is rapidly converted to 4,5-ddh-JA (Chini
425 et al., 2018) (see below).

426 The induction of sulfur assimilation and GSH production by OPDA were attributed as
427 specific signaling functions of OPDA (Park et al., 2013). Here, the transcriptional activation of

428 sulfur metabolism pathway was exclusive to the exogenous OPDA supply, contradicting an
429 intrinsic signaling function of the endogenous OPDA (Figure 4). As an electrophilic species,
430 OPDA was shown to disturb redox homeostasis (Mueller and Berger, 2009) and to inhibit
431 photosynthesis by affecting the photosystem II fluorescence (Alméras et al., 2003; Mueller et al.,
432 2008). In parallel, the *in planta* conjugation of OPDA to GSH, which is an important antioxidant
433 substance, and its degradation in the vacuole were also demonstrated (Ohkama-Ohtsu et al., 2011).
434 Taken together, this implies that OPDA may not directly regulate the sulfur assimilation pathway
435 but instead triggers this response through its potential detoxification when exogenously applied to
436 plants.
437

438 **Endogenously formed OPDA is sequestered to the organelles of JA biosynthesis**

439 To address the question whether OPDA remains sequestered in the plastids or whether it is
440 converted to 4,5-ddh-JA, a trans-organellar complementation approach was performed by directing
441 OPR3 into various organelles (Figure 5, Supplemental Figs. 7, 8). Occurrence of OPR3 in any of
442 the tested organelles resulted in a complementation of the phenotype and JA/JA-Ile production
443 upon wounding in *opr2opr3* mutants. This led to the assumption that OPDA might travel
444 throughout the cell. Nevertheless, the possibility still exists that OPDA is translocated directly to
445 the peroxisomes, where it is converted to 4,5-ddh-JA by β-oxidation as shown previously for *opr3*
446 and *opr2opr3* (Chini et al., 2018). Given that OPR3 is able to convert 4,5-ddh-JA to JA and OPDA
447 to OPC-8 *in vitro* (Supplemental Figure 9), the complementation approach with OPR3 could not
448 discriminate between the presence of either OPDA or 4,5-ddh-JA outside of the plastids or the
449 peroxisomes. To address this, organelle variants of the isoenzymes OPR2 and OPR1 were used to
450 complement the *opr2opr3* mutant (Figure 6). OPR2 and OPR1 differ in their enzymatic activity
451 against OPDA and 4,5-ddh-JA: OPR2 is able to convert both compounds, but OPR1 has been
452 shown to be inactive on 4,5-ddh-JA (Chini et al., 2018). Since OPDA and 4,5-ddh-JA should occur
453 in peroxisomes and possibly in the cytosol, reconstitution of JA biosynthesis was obtained using
454 either OPR1 or OPR2 targeted to peroxisomes or the cytosol. Targeting OPR1 or OPR2 to
455 mitochondria, however, discriminated whether OPDA or 4,5-ddh-JA is the substrate able to
456 translocate to other organelles (Figure 7). Here, complementation of *opr2opr3* with a
457 mitochondrial-located OPR1 did not rescue fertility and JA/JA-Ile production (Figure 6), whereas
458 OPR2 in mitochondria did. Additionally, OPR1 fully complemented the mutant only within the

459 peroxisome, and its cytosolic variant resulted in minimal JA-Ile formation and partial rescue of
460 fertility. These results suggest a restricted occurrence of OPDA in the cytosol and its preferred
461 compartmentalization in plastids and peroxisomes, whereas 4,5-ddh-JA might be the substrate able
462 to translocate between cell organelles.

463 In conclusion, despite its perception and signaling in lower plants, OPDA did not mediate
464 transcriptional changes in Arabidopsis. The induction of a specific transcriptional change occurred
465 exclusively upon exogenous supply but not upon endogenous rise of OPDA. The formation of JA-
466 Ile only by exogenous OPDA indicated that such an approach can introduce bias and suggested
467 that the endogenous OPDA is compartmentalized. The use of the trans-organellar complementation
468 approach to study the subcellular distribution of OPDA showed that OPR3 has specificity to other
469 JA precursors beside OPDA. When other OPR isoenzymes with higher substrate specificities were
470 used, the levels of restitution of JA-Ile biosynthesis in the mutant supported OPDA being limited
471 to the known organelles in the canonical pathway, while 4,5-ddh-JA was likely able to translocate
472 within the cell.

473

474

475 **Material and methods**

476 **Plant material, growth conditions, and treatment**

477 *Arabidopsis thaliana* wild type (ecotype Col-0) and the mutant lines *opr2opr3* (Chini et al., 2018)
478 and *aos* (*dde2-2*, von Malek et al., 2002) were genotyped using the primers listed (Supplemental
479 Table 2). After surface sterilization with 4% bleach and three-day stratification at 4°C, seedlings
480 were grown for ten days in liquid Murashige and Skoog (MS) medium (pH 5.7, 1% sucrose),
481 whereas adult plants were grown for four weeks in individual pots containing steam-sterilized clay,
482 coir fiber, and vermiculite. Plant growth took place in Phytocabinets (Percival Scientific,
483 www.percival-scientific.com/) at 120 µE $m^{-2}$ $s^{-1}$ under short day conditions (10/14 hours light/dark
484 cycle) at 21/19 °C and 65% relative humidity. For wounding, seedlings were squeezed with forceps
485 with serrated teeth. Phytohormone treatments were done by adding either 25 µM OPDA (≥ 95%,
486 Cayman Chemical, www.caymanchem.com) or 1 µM MeJA to the medium.

487 **RNA isolation, RNA-seq and quantitative RT-PCR analysis**

488 Total RNA was isolated from homogenized frozen material using the RNeasy Plant Mini Kit
489 (Qiagen) and treated with the DNA-free™ DNA Removal Kit (Invitrogen, #AM1906). First strand
490 cDNA synthesis from 1 µg DNA-free RNA was carried out using the RevertAid H Minus reverse
491 transcriptase with oligo(dT)18 primers (ThermoFisher Scientific™, www.thermofisher.com).
492 Quantitative PCR was carried-out in Hard-Shell® 96-Well PCR Plates (Bio-Rad Laboratories,
493 www.bio-rad.com, #HSP9601) supplied with 10 µL reaction mix of 1.5 ng/µL cDNA, 1x EvaGreen
494 QPCR Mix II (Bio&Sell, www.bio-sell.de, #BS76.580.0200) and 0.2 µM of forward and reverse
495 primers (Supplemental Table 2). The reactions were run on a CFX Connect Real-Time PCR
496 Detection System (Bio-Rad Laboratories) with denaturation (95°C for 15 min), amplification (40
497 cycles of 95°C for 15 s and 60°C for 30 s) and melt curve analysis (95°C for 10 s, 65°C heating up
498 to 95°C with a heating rate of 0.05°C $s^{-1}$). Gene expression was normalized to the housekeeping
499 gene *PROTEIN PHOSPHATASE 2A SUBUNIT A3* (AT1G13320) (Czechowski et al., 2005; Wang
500 et al., 2014) using the $2^{-\Delta CT}$ method (Schmittgen and Livak, 2008) and included biological
501 triplicates.

502 **Transcriptome analysis**

503 RNA quality and integrity were assessed on Agilent 2100 Bioanalyzer system (Agilent
504 Technologies, www.agilent.com) using the RNA 6000 Nano Kit for standard RNA sensitivity
505 (Agilent, #5067-1511). Three biological replicates were submitted to Novogene
506 (www.novogene.com) for mRNA paired-end short-read sequencing (150 bp length) on an Illumina
507 NovaSeq 6000 Sequencing System and bioinformatics analysis according to their pipeline. Reads
508 were mapped to the *A. thaliana* TAIR10 reference genome. Gene expression levels were
509 determined using the FPKM (Fragments per kilobase per million) method. Gene expression
510 heatmaps, principal component analysis (PCA), gene clustering, and Gene Ontology (GO)
511 enrichment analysis, were generated using the iDEP .96 and iDEP 1.1 software tools (Ge et al.,
512 2018).

513 **Protein extraction and immunoblotting**

514 Proteins were extracted by incubation of 50 mg frozen material in 200 µl of extraction buffer (25
515 mM Tris-Cl pH 6.8, 1% SDS, 1% [v/v] β-mercaptoethanol) at 95°C for ten minutes. Extracts were
516 treated with 1% (v/v) Halt™ Protease and Phosphatase Inhibitor Cocktail (ThermoFisher
517 Scientific™, #78440) and quantified at 595 nm on the SPARK® multimode microplate reader
518 (TECAN) using the Pierce™ Bradford Plus Protein Assay Kit (ThermoFisher Scientific™,

519 #23236). Ten micrograms of total protein were incubated at 96°C for 10 min in Laemmli Buffer
520 (1:1, (Laemmli, 1970) to dissolve AOC trimers (Otto et al., 2016). Proteins were separated on
521 SDS–PAGE (4% and 12% acrylamide for stacking and resolving gels, respectively), transferred to
522 a PVDF membrane and detected using Ponceau S staining or No-Stain™ Protein Labeling Reagent
523 (ThermoFisher Scientific™, #A44449). Membrane blocking in 5% (w/v) BSA in TBST (20 mM
524 Tris–Cl pH 7.8, 150 mM NaCl, 0.05% [v/v] Tween) was followed by immuno-staining using anti-
525 AtAOC primary antibody (1:5000, Stenzel et al., 2003) and a goat anti-rabbit IgG secondary
526 antibody conjugated with alkaline phosphatase (1:4000, Chemicon®, Sigma-Aldrich,
527 www.sigmaaldrich.com, #AP307P). Detection by chemiluminescence with Immun-Star AP
528 Substrate (ThermoFisher Scientific, #1705018) was visualized using a Fusion FX Imaging system
529 (Vilber, www.vilber.com). AOC protein bands were quantified relative to total protein loadings
530 using densitometry analysis with ImageJ (https://imagej.nih.gov/ij/index.html).

531 **Cloning of the OPRs and plant transformation**

532 The OPR3 (1176 bp), OPR2 (1125 bp), and OPR1 (1194 bp) coding sequences (CDS) without stop
533 codons were PCR-amplified from Col-0 cDNA using the Q5® High-Fidelity DNA Polymerase
534 (Bio Labs, www.biolabs.io, #M0491) and the listed primer pairs (Supplemental Table 3). For
535 OPR3ΔSRL, the last nine nucleotides were removed, and silent mutations C205G and G1109C
536 were introduced to eliminate *BsaI* and *BpiI* sites, respectively. The CDS were cloned into the
537 Golden Gate level 0 vectors pAGM1287 and pAGM1299 (Engler et al., 2014). OPR fusions to
538 YFP were generated by in-frame assembly of the level 0 with YFP at the C-terminus connected by
539 a Gly-Ser linker. The final cloning cassettes containing the CaMV *35S* promoter and *tOcs*
540 terminator in addition to the Oleosin-RFP plant selection marker were assembled in the
541 pAGM55171 vector.
542 Plant stable transformation was carried-out by floral dip with *Agrobacterium tumefaciens* strain
543 *GV3101* according to (Zhang et al., 2006). To circumvent the *opr2opr3* mutant sterility, MeJA was
544 applied to flower buds from 48 hours post-dipping until the first silique formation. Transformant
545 selection relied on the seed coat RFP marker and single-insertion lines were identified by
546 segregation analysis determining the ratio of fluorescent to non-fluorescent seeds.

547 **Subcellular targeting of the OPRs**

548 Organelle variants of OPR3, OPR2, and OPR1 were generated by adding organelle targeting
549 signals to the N- and/or C-terminal regions of the OPRs and/or YFP sequences (Supplemental
550 Table 1). For nuclear targeting, OPR3ΔSRL was fused to the nuclear localization signal from
551 Simian Virus 40 (Lu et al., 2021; Raikhel, 1992), while its targeting to the cytosol relied on a C-
552 terminal nuclear export signal from the HIV1 REV (Kosugi et al., 2008). ER-localized OPR3ΔSRL
553 was generated by flanking the sequence between an N-terminal signal peptide from the AtCAPE3
554 (Kunze and Berger, 2015) and a C-terminal HDEL retention signal (De Meyer and Depicker,
555 2014). Import to the chloroplast stroma and mitochondria, relied on an N-terminal target peptide
556 from the AtRECA1 (Eseverri et al., 2020) and the Rieske protein (von Heijne et al., 1989),
557 respectively.

558 **Transient expression in *N. benthamiana* leaves and protoplasts.**

559 *A. tumefaciens* strain *GV3101*, harboring OPR constructs, was cultured for 48 hours in LB medium
560 with the appropriate antibiotics. The bacteria were syringe-infiltrated into *N. benthamiana* leaves
561 according to (Norkunas et al., 2018). Leaf disc imaging was performed 48-72 hours post-
562 infiltration.
563 Protoplasts were isolated from leaves of 4-week-old *N. benthamiana* plants, as described (Janik et
564 al., 2019). Isolated protoplasts were co-transfected with level 1 plasmids of OPR3 constructs and
565 organelle markers (Stellmach et al., 2022) using a mixture of 200 µl of protoplast suspension and
566 10 µg of DNA. Protoplasts were incubated at room temperature overnight after PEG-
567 transformation and used for imaging.

568 **Confocal microscopy**
569 Confocal microscopy utilized LSM880 and LSM900 laser scanning microscopes (Zeiss Germany,
570 www.zeiss.de). Fluorophores were excited with 514 nm (YFP) and 561 nm (mCherry) laser lines
571 and detected at 510–560 nm and 570-650 nm, respectively. Image acquisition and processing were
572 performed using ZEN software (version 3.4, 2021, Zeiss).

573 **Phytohormone measurements**
574 Measurements of OPDA, *dn*-OPDA, JA, and JA-Ile were performed using a standardized Ultra-
575 performance liquid chromatography–tandem Mass Spectrometry (UPLC– MS/MS)-based method
576 (Balcke et al., 2012). 50 mg of powdered frozen tissue were extracted with 500 µl 100% LC-MS
577 methanol supplemented with 50 ng of [$^{2}H_{5}$]OPDA, [$^{2}H_{6}$]JA, and [$^{2}H_{2}$]JA-Ile each as internal

578 standards. After solid-phase extraction on HR-XC (Chromabond, Macherey-Nagel, www.mn-
579 net.com), 10 µl of the eluate were analyzed via UPLC–MS/MS, and analyte content was
580 determined relative to the internal standard peak heights. *dn*-OPDA content was determined using
581 [$^{2}H_{5}$]OPDA as the internal standard.

582 **Determination of enzymatic activity of OPR3**

583 OPR3 CDS inserted in pET28a(+) with *EcoR*I and *Not*I cloning sites was ordered from BioCat
584 GmbH (www.biocat.com) and transformed into *Escherichia coli* BL21 Star (DE3) cells
585 (ThermoFisher Scientific) by heat shock. Protein expression was performed in auto-induction
586 medium at 16°C for three days (Studier, 2005). Harvested cells were resolved in buffer HisA
587 (50 mM Tris/HCl pH 7.8, 100 mM NaCl, 10% (v/v) glycerol, 2 mM $MgCl_2$ and 5 mM imidazole)
588 supplemented with lysozyme, DNAse I and 0.2 mM PMSF. After a 30-minute incubation on ice,
589 cells were sonicated and cleared lysate was applied to 1 mL HisTrap FastFlow column (Cytiva,
590 www.cytivalifesciences.com). Protein was eluted with buffer HisB (50 mM Tris/HCl pH 7.8,
591 100 mM NaCl, 10% (v/v) glycerol, 2 mM $MgCl_2$ and 500 mM imidazole), which was changed to
592 storage buffer (50 mM Tris/HCl pH 7.8, 100 mM NaCl, 10% (v/v) glycerol, 2 mM $MgCl_2$) by
593 dialysis (MWCO 12-14 kDa) at 4°C overnight. Following SDS-PAGE, protein fractions were used
594 for *in vitro* assays at 0.1 mg/mL together with 0.05 mM substrate, 1 mM NADPH and 10 mM NaCl
595 in 20 mM Tris/HCl pH 7.8. Reactions were incubated at 30°C for 10 minutes and stopped by one
596 volume acetonitrile. Enzyme deactivated by one volume acetonitrile was used as control. Assays
597 were analyzed via UHPLC-high resolution (HR)-MS according to Feussner et al. (2023). Data was
598 analyzed using the MassHunter Qualitative Analysis 10.0 software (Agilent Technologies).

599 **Figures and statistical analysis**

600 Micrographs and photographs were processed through PHOTOSHOP 12.0.4 (Adobe Systems,
601 http://www.adobe.com). The statistical analyses applied to the different datasets were performed
602 using GraphPad Prism (www.graphpad.com).

603

604

605

606 **Data availability**

607 The datasets generated and/or analyzed during this study are available from the corresponding
608 author on request. Transcriptomic raw data were deposited in Sequence Read Archive (SRA) of
609 NCBI (PRJNA1088739).

610

611 **Funding**

612 K.M. and B.H. were supported by the Deutsche Forschungsgemeinschaft (DFG, German Research
613 Foundation) grant No 400681449/GRK2498. M.K. was supported by the DFG grant No
614 273134146/GRK 2172. I.F. acknowledges funding from the DFG (GRK 2172-PRoTECT, INST
615 186/1434-1, and ZUK 45/2010).

616

617 **Author contributions**

618 Conceptualization, B.H and K.M.; Methodology, K.M, R.B, and F.S.; Investigation, K.M., R.B.,
619 F.S., and M.K.; Analyzing Data, I.F. and B.H.; Writing – Original Draft, K.M.; Writing – Review
620 & Editing, B.H. and I.F.; Funding Acquisition, B.H. and I.F.;

621

622 **Acknowledgments**

623 We thank Hagen Stellmach (IPB Halle, Germany) for help in jasmonate quantification, Andreas
624 Schaller (University of Hohenheim, Germany) and Mats Hamberg (Karolinska Institute, Sweden)
625 for providing seeds of *opr2opr3* and 4,5-ddh-JA, respectively. We thank Sylvestre Marillonnet
626 (IPB Halle) for providing the Golden Gate modules and vectors used in this study. Khabat Vahabi
627 (IPB Halle) is acknowledged for assistance in RNAseq preparation and data analysis Claus
628 Wasternack (IPB Halle) and Alain Tissier (IPB Halle) are acknowledged for critical reading of the
629 manuscript.

630

631 **Declaration of interests**

The authors declare no competing interests.

633 **References**


634 **Adhikari, A., and Park, S.-W.** (2023). Reduced GSH acts as a metabolic cue of OPDA signaling
635 in coregulating photosynthesis and defense activation under stress. Plants **12**:3745.

636 **Alméras, E., Stolz, S., Vollenweider, S., Reymond, P., Mène-Saffrané, L., and Farmer, E.**
637 (2003). Reactive electrophile species activate defense gene expression in Arabidopsis. Plant
638 J. **34**:205-216.

639 **Andreou, A., and Feussner, I.** (2009). Lipoxygenases - Structure and reaction mechanism.
640 Phytochemistry **70**:1504-1510.

641 **Balcke, G., Handrick, V., Bergau, N., Fichtner, M., Henning, A., Stellmach, H., Tissier, A.,**
642 **Hause, B., and Frolov, A.** (2012). An UPLC-MS/MS method for highly sensitive high-
643 throughput analysis of phytohormones in plant tissues. Plant Methods **8**:47.

644 **Bannenberg, G., Martínez, M., Hamberg, M., and Castresana, C.** (2009). Diversity of the
645 enzymatic activity in the lipoxygenase gene family of *Arabidopsis thaliana*. Lipids **44**:85-
646 95. 10.1007/s11745-008-3245-7.

647 **Browse, J.** (2009). The power of mutants for investigating jasmonate biosynthesis and signaling.
648 Phytochemistry **70**:1539-1546.

649 **Chang, Y., Shi, M., Sun, Y., Cheng, H., Ou, X., Zhao, Y., Zhang, X., Day, B., Miao, C., and**
650 **Jiang, K.** (2023). Light-induced stomatal opening in Arabidopsis is negatively regulated
651 by chloroplast-originated OPDA signaling. Curr. Biol. **33**:1071-1081.e1075.
652 https://doi.org/10.1016/j.cub.2023.02.012.

653 **Chini, A., Monte, I., Zamarreño, A.M., García-Mina, J.M., and Solano, R.** (2023). Evolution
654 of the jasmonate ligands and their biosynthetic pathways. New Phytol. **238**:2236-2246.
655 https://doi.org/10.1111/nph.18891.

656 **Chini, A., Fonseca, S., Fernandez, G., Adie, B., Chico, J.M., Lorenzo, O., Garcia-Casado, G.,**
657 **Lopez-Vidriero, I., Lozano, F.M., Ponce, M.R., et al.** (2007). The JAZ family of
658 repressors is the missing link in jasmonate signalling. Nature **448**:666-671.

659 **Chini, A., Monte, I., Zamarreño, A.M., Hamberg, M., Lassueur, S., Reymond, P., Weiss, S.,**
660 **Stintzi, A., Schaller, A., Porzel, A., et al.** (2018). An OPR3-independent pathway uses
661 4,5-didehydrojasmonate for jasmonate synthesis. Nature Chem. Biol. **14**:171.
662 10.1038/nchembio.2540.

663 **Chung, H.S., Koo, A.J.K., Gao, X., Jayanty, S., Thines, B., Jones, A.D., and Howe, G.A.**
664 (2008). Regulation and function of Arabidopsis *JASMONATE ZIM*-domain genes in
665 response to wounding and herbivory. Plant Physiol. **146**:952-964.
666 **Czechowski, T., Stitt, M., Altmann, T., Udvardi, M.K., and Scheible, W.-R.** (2005). Genome-
667 wide identification and testing of superior reference genes for transcript normalization in
668 Arabidopsis. Plant Physiol. **139**:5-17. 10.1104/pp.105.063743.
669 **Dave, A., and Graham, I.A.** (2012). Oxylipin signalling: a distinct role for the jasmonic acid
670 precursor *cis*-(+)-12-oxo-phytodienoic acid (*cis*-OPDA). Front. Plant Sci.
671 **3:42**10.3389/fpls.2012.00042.
672 **Dave, A., Hernández, M.L., He, Z., Andriotis, V.M.E., Vaistij, F.E., Larson, T.R., and**
673 **Graham, I.A.** (2011). 12-Oxo-phytodienoic acid accumulation during seed development
674 represses seed germination in Arabidopsis. Plant Cell **23**:583-599. 10.1105/tpc.110.081489.
675 **Davletova, S., Schlauch, K., Coutu, J., and Mittler, R.** (2005). The Zinc-Finger Protein Zat12
676 plays a central role in reactive oxygen and abiotic stress signaling in Arabidopsis Plant
677 Physiol. **139**:847-856. 10.1104/pp.105.068254.
678 **Davoine, C., Falletti, O., Douki, T., Iacazio, G., Ennar, N., Montillet, J.-L., and**
679 **Triantaphylides, C.** (2006). Adducts of oxylipin electrophiles to glutathione reflect a 13
680 specificity of the downstream lipoxygenase pathway in the tobacco hypersensitive
681 response. Plant Physiol. **140**:1484-1493.
682 **De Meyer, T., and Depicker, A.** (2014). Trafficking of endoplasmic reticulum-retained
683 recombinant proteins is unpredictable in *Arabidopsis thaliana*. Front. Plant Sci.
684 **5**10.3389/fpls.2014.00473.
685 **Delessert, C., Wilson, I., Straeten, D., Dennis, E., and Dolferus, R.** (2004). Spatial and temporal
686 analysis of the local response to wounding. Plant Mol. Biol. **55**:165-181.
687 **Engler, C., Youles, M., Gruetzner, R., Ehnert, T.-M., Werner, S., Jones, J.D.G., Patron, N.J.,**
688 **and Marillonnet, S.** (2014). A Golden Gate modular cloning toolbox for plants. ACS
689 Synthetic Biol. **3**:839-843. 10.1021/sb4001504.
690 **Eseverri, Á., Baysal, C., Medina, V., Capell, T., Christou, P., Rubio, L.M., and Caro, E.**
691 (2020). Transit peptides from photosynthesis-related proteins mediate import of a marker
692 protein into different plastid types and within different species. Front. Plant Sci.
693 **11**10.3389/fpls.2020.560701.

694 **Feussner, I., and Wasternack, C.** (2002). The lipoxygenase pathway. Annu. Rev. Plant Biol.
695 **53**:275-297.
696 **Feussner, K., Abreu, I.N., Klein, M., and Feussner, I.** (2023). Chapter twelve - metabolite
697 fingerprinting: A powerful metabolomics approach for marker identification and functional
698 gene annotation. In Methods Enzymol., J. Jez, ed. (Academic Press: pp. 325-350.
699 https://doi.org/10.1016/bs.mie.2022.08.015.
700 **Ge, S.X., Son, E.W., and Yao, R.** (2018). iDEP: an integrated web application for differential
701 expression and pathway analysis of RNA-Seq data. BMC Bioinformatics **19**:534.
702 10.1186/s12859-018-2486-6.
703 **Goetz, S., Hellwege, A., Stenzel, I., Kutter, C., Hauptmann, V., Forner, S., McCaig, B., Hause,**
704 **G., Miersch, O., Wasternack, C., et al.** (2012). Role of cis-12-oxo-phytodienoic acid in
705 tomato embryo development. Plant Physiol. **158**:1715-1727. 10.1104/pp.111.192658.
706 **Goodspeed, D., Chehab, E.W., Min-Venditti, A., Braam, J., and Covington, M.F.** (2012).
707 Arabidopsis synchronizes jasmonate-mediated defense with insect circadian behavior.
708 Proc. Natl. Acad. Sci. USA **109**:4674-4677. 10.1073/pnas.1116368109.
709 **Gould, S.J., Keller, G.A., Hosken, N., Wilkinson, J., and Subramani, S.** (1989). A conserved
710 tripeptide sorts proteins to peroxisomes. J. Cell Biol. **108**:1657-1664.
711 10.1083/jcb.108.5.1657.
712 **Guo, Q., Yoshida, Y., Major, I.T., Wang, K., Sugimoto, K., Kapali, G., Havko, N.E., Benning,**
713 **C., and Howe, G.A.** (2018). JAZ repressors of metabolic defense promote growth and
714 reproductive fitness in *Arabidopsis*. Proc. Natl. Acad. Sci. USA **115**:E10768-E10777.
715 10.1073/pnas.1811828115.
716 **Howe, G.A.** (2004). Jasmonates as signals in the wound response. J. Plant Growth Regul. **23**:223-
717 237.
718 **Janik, K., Stellmach, H., Mittelberger, C., and Hause, B.** (2019). Characterization of
719 phytoplasmal effector protein interaction with proteinaceous plant host targets using
720 bimolecular fluorescence complementation (BiFC). In Phytoplasmas: Methods and
721 Protocols, R. Musetti and L. Pagliari, eds. (Springer New York: New York, NY), pp. 321-
722 331. 10.1007/978-1-4939-8837-2_24
723 **Jimenez-Aleman, G.H., Thirumalaikumar, V.P., Jander, G., Fernie, A.R., and Skirycz, A.**
724 (2022). OPDA, more than just a jasmonate precursor. Phytochemistry **204**:113432.
725 https://doi.org/10.1016/j.phytochem.2022.113432.

726 **Koo, A.J.K., and Howe, G.A.** (2009). The wound hormone jasmonate. Phytochemistry **70**:1571-
727 1580.
728 **Kosugi, S., Hasebe, M., Tomita, M., and Yanagawa, H.** (2008). Nuclear export signal consensus
729 sequences defined using a localization-based yeast selection system. Traffic **9**:2053-2062.
730 https://doi.org/10.1111/j.1600-0854.2008.00825.x.
731 **Kunze, M., and Berger, J.** (2015). The similarity between N-terminal targeting signals for protein
732 import into different organelles and its evolutionary relevance. Front. Physiol.
733 **6**10.3389/fphys.2015.00259.
734 **Laemmli, U.K.** (1970). Cleavage of structural proteins during the assembly of the head of
735 bacteriophage T4. Nature **227**:680-685.
736 **Lewandowska, M., Zienkiewicz, A., Feussner, K., König, S., Kunst, L., and Feussner, I.**
737 (2023). Wound-induced triacylglycerol biosynthesis is jasmonoy-l-isoleucin and abscisic
738 acid independent. Plant Biol. **25**:509-517. https://doi.org/10.1111/plb.13513.
739 **Li, C., Xu, M., Cai, X., Han, Z., Si, J., and Chen, D.** (2022). Jasmonate signaling pathway
740 modulates plant defense, growth, and their trade-offs. Int. J. Mol. Sci. **23**:3945.
741 **Liu, W., and Park, S.-W.** (2021). 12-oxo-Phytodienoic acid: A fuse and/or switch of plant growth
742 and defense responses? Front. Plant Sci. **12**10.3389/fpls.2021.724079.
743 **Lu, J., Wu, T., Zhang, B., Liu, S., Song, W., Qiao, J., and Ruan, H.** (2021). Types of nuclear
744 localization signals and mechanisms of protein import into the nucleus. Cell Comm. Signal.
745 **19**:60. 10.1186/s12964-021-00741-y.
746 **Mehrshahi, P., Stefano, G., Andaloro, J.M., Brandizzi, F., Froehlich, J.E., and DellaPenna,**
747 **D.** (2013). Transorganellar complementation redefines the biochemical continuity of
748 endoplasmic reticulum and chloroplasts. Proc. Natl. Acad. Sci. USA **110**:12126-12131.
749 10.1073/pnas.1306331110.
750 **Mittler, R., Kim, Y., Song, L., Coutu, J., Coutu, A., Ciftci-Yilmaz, S., Lee, H., Stevenson, B.,**
751 **and Zhu, J.-K.** (2006). Gain- and loss-of-function mutations in Zat10 enhance the
752 tolerance of plants to abiotic stress. FEBS Lett. **580**:6537-6542.
753 https://doi.org/10.1016/j.febslet.2006.11.002.
754 **Mizoi, J., Kanazawa, N., Kidokoro, S., Takahashi, F., Qin, F., Morimoto, K., Shinozaki, K.,**
755 **and Yamaguchi-Shinozaki, K.** (2019). Heat-induced inhibition of phosphorylation of the
756 stress-protective transcription factor DREB2A promotes thermotolerance of *Arabidopsis*
757 *thaliana*. J. Biol. Chem. **294**:902-917. https://doi.org/10.1074/jbc.RA118.002662.

758 **Monte, I., Caballero, J., Zamarreño, A.M., Fernández-Barbero, G., García-Mina, J.M., and**
759 **Solano, R.** (2022). JAZ is essential for ligand specificity of the COI1/JAZ co-receptor.
760 Proc. Natl. Acad. Sci. USA **119**:e2212155119. doi:10.1073/pnas.2212155119.
761 **Monte, I., Kneeshaw, S., Franco-Zorrilla, J.M., Chini, A., Zamarreño, A.M., García-Mina,**
762 **J.M., and Solano, R.** (2020). An ancient COI1-independent function for reactive
763 electrophilic oxylipins in thermotolerance. Curr. Biol. **30**:962-971.e963.
764 10.1016/j.cub.2020.01.023.
765 **Monte, I., Ishida, S., Zamarreño, A.M., Hamberg, M., Franco-Zorrilla, J.M., García-Casado,**
766 **G., Gouhier-Darimont, C., Reymond, P., Takahashi, K., García-Mina, J.M., et al.**
767 (2018). Ligand-receptor co-evolution shaped the jasmonate pathway in land plants. Nature
768 Chem. Biol. **14**:480-488. 10.1038/s41589-018-0033-4.
769 **Mueller, M.J., and Berger, S.** (2009). Reactive electrophilic oxylipins: Pattern recognition and
770 signalling. Phytochemistry **70**:1511-1521.
771 **Mueller, S., Hilbert, B., Dueckershoff, K., Roitsch, T., Krischke, M., Mueller, M.J., and**
772 **Berger, S.** (2008). General detoxification and stress responses are mediated by oxidized
773 lipids through TGA transcription factors in *Arabidopsis*. Plant Cell **20**:768-785.
774 **Müller, S.M., Wang, S., Telman, W., Liebthal, M., Schnitzer, H., Viehhauser, A., Sticht, C.,**
775 **Delatorre, C., Wirtz, M., Hell, R., et al.** (2017). The redox-sensitive module of cyclophilin
776 20-3, 2-cysteine peroxiredoxin and cysteine synthase integrates sulfur metabolism and
777 oxylipin signaling in the high light acclimation response. Plant J. **91**:995-1014.
778 10.1111/tpj.13622.
779 **Norkunas, K., Harding, R., Dale, J., and Dugdale, B.** (2018). Improving agroinfiltration-based
780 transient gene expression in *Nicotiana benthamiana*. Plant Methods **14**:71.
781 10.1186/s13007-018-0343-2.
782 **Ohkama-Ohtsu, N., Sasaki-Sekimoto, Y., Oikawa, A., Jikumaru, Y., Shinoda, S., Inoue, E.,**
783 **Kamide, Y., Yokoyama, T., Hirai, M.Y., Shirasu, K., et al.** (2011). 12-Oxo-phytodienoic
784 acid-glutathione conjugate is transported into the vacuole in Arabidopsis. Plant Cell
785 Physiol. **52**:205-209.
786 **Otto, M., Naumann, C., Brandt, W., Wasternack, C., and Hause, B.** (2016). Activity regulation
787 by heteromerization of Arabidopsis allene oxide cyclase family members. Plants **5**:3.
788 **Park, S.-W., Li, W., Viehhauser, A., He, B., Kim, S., Nilsson, A.K., Andersson, M.X., Kittle,**
789 **J.D., Ambavaram, M.M.R., Luan, S., et al.** (2013). Cyclophilin 20-3 relays a 12-oxo-

790 phytodienoic acid signal during stress responsive regulation of cellular redox homeostasis.
791 Proc. Natl. Acad. Sci. USA **110**:9559-9564. 10.1073/pnas.1218872110.
792 **Pollmann, S., Springer, A., Rustgi, S., von Wettstein, D., Kang, C., Reinbothe, C., and**
793 **Reinbothe, S.** (2019). Substrate channeling in oxylipin biosynthesis through a protein
794 complex in the plastid envelope of *Arabidopsis thaliana*. J. Exper. Bot. **70**:1483-1495.
795 10.1093/jxb/erz015.
796 **Raikhel, N.** (1992). Nuclear targeting in plants 1. Plant Physiol. **100**:1627-1632.
797 10.1104/pp.100.4.1627.
798 **Reymond, P., Weber, H., Damond, M., and Farmer, E.** (2000). Differential gene expression in
799 response to mechanical wounding and insect feeding in Arabidopsis. Plant Cell **12**:707-719.
800 **Ribot, C., Zimmerli, C., Farmer, E.E., Reymond, P., and Poirier, Y.** (2008). Induction of the
801 Arabidopsis *PHO1;H10* gene by 12-oxo-phytodienoic acid but not jasmonic acid via a
802 *CORONATINE INSENSITIVE1*-dependent pathway. Plant Physiol. **147**:696-706.
803 **Sakuma, Y., Maruyama, K., Qin, F., Osakabe, Y., Shinozaki, K., and Yamaguchi-Shinozaki,**
804 **K.** (2006). Dual function of an *Arabidopsis* transcription factor DREB2A in water-stress-
805 responsive and heat-stress-responsive gene expression. Proc. Natl. Acad. Sci. USA
806 **103**:18822-18827. doi:10.1073/pnas.0605639103.
807 **Savchenko, T., and Dehesh, K.** (2014). Drought stress modulates oxylipin signature by eliciting
808 12-OPDA as a potent regulator of stomatal aperture. Plant Signal. Behavior **9**:e28304.
809 **Schaller, A., and Stintzi, A.** (2009). Enzymes in jasmonate biosynthesis - Structure, function,
810 regulation. Phytochemistry **70**:1532-1538.
811 **Schaller, F., Biesgen, C., Müssig, C., Altmann, T., and Weiler, E.W.** (2000). 12-
812 Oxophytodienoate reductase 3 (OPR3) is the isoenzyme involved in jasmonate
813 biosynthesis. Planta **210**:979-984.
814 **Schmittgen, T.D., and Livak, K.J.** (2008). Analyzing real-time PCR data by the comparative
815 C(T) method. Nature Protocols **3**:1101-1108.
816 **Sheard, L.B., Tan, X., Mao, H., Withers, J., Ben-Nissan, G., Hinds, T.R., Kobayashi, Y., Hsu,**
817 **F.-F., Sharon, M., Browse, J., et al.** (2010). Jasmonate perception by inositol-phosphate-
818 potentiated COI1-JAZ co-receptor. Nature **468**:400-405.
819 **Stellmach, H., Hose, R., Räde, A., Marillonnet, S., and Hause, B.** (2022). A new set of Golden-
820 Gate-based organelle marker plasmids for colocalization studies in plants. Plants **11**:2620.

821 **Stelmach, B.A., Müller, A., Hennig, P., Laudert, D., Andert, L., and Weiler, E.W.** (1998).
822 Quantitation of the octadecanoid 12-oxo-phytodienoic acid, a signalling compound in plant
823 mechanotransduction. Phytochemistry **47**:539-546.
824 **Stenzel, I., Hause, B., Miersch, O., Kurz, T., Maucher, H., Weichert, H., Ziegler, J., Feussner,**
825 **I., and Wasternack, C.** (2003). Jasmonate biosynthesis and the allene oxide cyclase family
826 of *Arabidopsis thaliana*. Plant Mol. Biol. **51**:895-911.
827 **Stintzi, A., and Browse, J.** (2000). The Arabidopsis male-sterile mutant, *opr3*, lacks the 12-
828 oxophytodienoic acid reductase required for jasmonate synthesis. Proc. Natl. Acad. Sci.
829 USA **97**:10625-10630.
830 **Stintzi, A., Weber, H., Reymond, P., Browse, J., and Farmer, E.** (2001). Plant defense in the
831 absence of jasmonic acid: The role of cyclopentanones. Proc. Natl. Acad. Sci. USA
832 **98**:12837-12842.
833 **Studier, F.W.** (2005). Protein production by auto-induction in high density shaking cultures.
834 Protein Expr. Purif. **41**:207-234. 10.1016/j.pep.2005.01.016.
835 **Taki, N., Sasaki-Sekimoto, Y., Obayashi, T., Kikuta, A., Kobayashi, K., Ainai, T., Yagi, K.,**
836 **Sakurai, N., Suzuki, H., Masuda, T., et al.** (2005). 12-oxo-phytodienoic acid triggers
837 expression of a distinct set of genes and plays a role in wound-induced gene expression in
838 Arabidopsis. Plant Physiol. **139**:1268-1283.
839 **Thines, B., Katsir, L., Melotto, M., Niu, Y., Mandaokar, A., Liu, G., Nomura, K., He, S.Y.,**
840 **Howe, G.A., and Browse, J.** (2007). JAZ repressor proteins are targets of the $SCF^{COI1}$
841 complex during jasmonate signalling. Nature **448**:661-665.
842 **Verhage, A., Vlaardingerbroek, I., Raaijmakers, C., Van Dam, N., Dicke, M., Van Wees,**
843 **S.C.M., and Pieterse, C.M.J.** (2011). Rewiring of the jasmonate signaling pathway in
844 Arabidopsis during insect herbivory. Front. Plant Sci. **2**10.3389/fpls.2011.00047.
845 **von Heijne, G., Steppuhn, J., and Herrmann, R.G.** (1989). Domain structure of mitochondrial
846 and chloroplast targeting peptides. Europ. J. Biochem. **180**:535-545.
847 https://doi.org/10.1111/j.1432-1033.1989.tb14679.x.
848 **von Malek, B., van der Graaff, E., Schneitz, K., and Keller, B.** (2002). The Arabidopsis male-
849 sterile mutant *dde2-2* is defective in the *ALLENE OXIDE SYNTHASE* gene encoding one
850 of the key enzymes of the jasmonic acid biosynthesis pathway. Planta **216**:187-192.

**Wang, H., Wang, J., Jiang, J., Chen, S., Guan, Z., Liao, Y., and Chen, F.** (2014). Reference genes for normalizing transcription in diploid and tetraploid Arabidopsis. Sci. Rep. **4**:6781. 10.1038/srep06781.

**Wang, J., Wu, D., Wang, Y., and Xie, D.** (2019). Jasmonate action in plant defense against insects. J. Exper. Bot. **70**:3391-3400. 10.1093/jxb/erz174.

**Wasternack, C.** (2006). Oxylipins: biosynthesis, signal transduction and action. In Plant Hormone Signaling, P. Hedden and S. Thomas, eds. (Blackwell Publishing: Harpenden), pp. 185-228.

**Wasternack, C.** (2019). New light on local and systemic wound signaling. Trends Plant Sci. **24**:102-105. https://doi.org/10.1016/j.tplants.2018.11.009.

**Wasternack, C., and Hause, B.** (2013). Jasmonates: biosynthesis, perception, signal transduction and action in plant stress response, growth and development. An update to the 2007 review in Annals of Botany. Ann. Bot. **111**:1021-1058. 10.1093/aob/mct067.

**Wasternack, C., and Strnad, M.** (2016). Jasmonate signaling in plant stress responses and development – active and inactive compounds. New Biotechnol. **33**:604-613. http://dx.doi.org/10.1016/j.nbt.2015.11.001.

**Weber, H., Vick, B., and Farmer, E.** (1997). Dinor-oxo-phytodienoic acid: A new hexadecanoid signal in the jasmonate family. Proc. Natl. Acad. Sci. USA **94**:10473-10478.

**Xie, D.-X., Feys, B., James, S., Nieto-Rostro, M., and Turner, J.** (1998). COI1: An Arabidopsis gene required for jasmonate-regulated defense and fertility. Science **280**:1091-1094.

**Xu, L., Liu, F., Lechner, E., Genschik, P., Crosby, W., Ma, H., Peng, W., Huang, D., and Xie, D.** (2002). The SCF-coi1 ubiquitin-ligase complexes are required for jasmonate response in Arabidopsis. Plant Cell **14**:1919-1935.

**Yan, J., Yao, R., Chen, L., Li, S., Gu, M., Nan, F., and Xie, D.** (2018). Dynamic perception of jasmonates by the F-box protein COI1. Mol. Plant **11**:1237-1247. 10.1016/j.molp.2018.07.007.

**Zhang, G., Liu, W., Gu, Z., Wu, S., E, Y., Zhou, W., Lin, J., and Xu, L.** (2023). Roles of the wound hormone jasmonate in plant regeneration. J. Exper. Bot. **74**:1198-1206. 10.1093/jxb/erab508.

**Zhang, X., Henriques, R., Lin, S.-S., Niu, Q.-W., and Chua, N.-H.** (2006). *Agrobacterium*-mediated transformation of *Arabidopsis thaliana* using the floral dip method. Nature Protocols **1**:641-646. 10.1038/nprot.2006.97.

882 **Supplemental data**

883

884 **Figure S1**: Seedlings of *opr2opr3* mutant show diminished AOC proteins content and produce
885 lower OPDA levels compared to wild type (Col-0).
886 **Figure S2**: The experimental setup for transcriptome analyses.
887 **Figure S3**: Hierarchical clustering and principal component analysis (PCA) illustrating the wound-
888 induced transcriptional changes in Col-0, *opr2opr3* and *aos*.
889 **Figure S4**: The JA-dependent wound response occurring in wild type seedlings.
890 **Figure S5**: Clustering of the transcriptional response of seedlings from *opr2opr3* upon treatment
891 with 25 µM OPDA with the response of seedlings from Col-0, *opr2opr3* and *aos* upon wounding.
892 **Figure S6**: The concept of the trans-organellar complementation of the *opr2opr3* mutant.
893 **Figure S7:** The removal of the SRL peroxisomal signal results in a cytosolic localization of OPR3
894 in *N. benthamiana* leaves and targeting of OPR3ΔSRL to the nucleus, cytosol, plastid stroma and
895 mitochondria in stable transformed *opr2opr3* lines.
896 **Figure S8**: OPR3 targeted to the ER, cytosol, nucleus, and chloroplasts colocalizes with the
897 corresponding organelle markers in *N. benthamiana* protoplasts.
898 **Figure S9**: OPR3 reduces OPDA and 4,5-ddh-JA *in vitro*.
899 **Figure S10**: OPDA levels at 1 h after wounding of seedlings of wild type (WT) or *opr2opr3*
900 transformed with either empty vector (EV), *35S::OPR2* or *35S::OPR1* targeted to peroxisomes
901 (Px), cytosol (Cyt) or mitochondria (Mt).

902

903 **Table S1:** Peptide sequences of the targeting signals used for subcellular targeting.
904 **Table S2:** Primers sequences used for mutants genotyping and RT-qPCR.
905 **Table S3:** Primer sequences used for Golden Gate cloning of OPR3, OPR2 and OPR1 and their
906 subcellular targeting.

907

## Figures

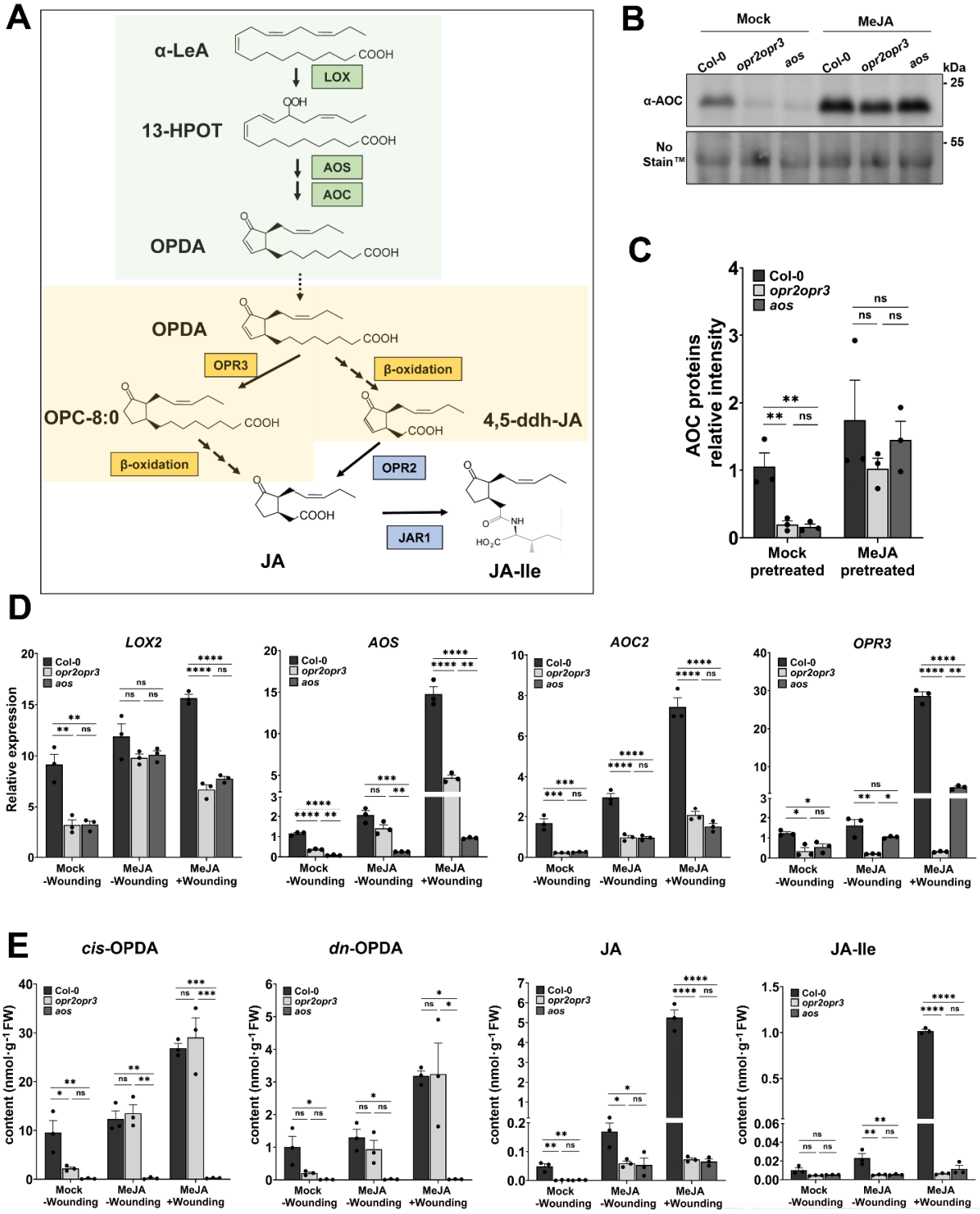
A
α-LeA
COOH
LOX
13-HPOT
OOH
COOH
AOS
AOC
OPDA
COOH
OPDA
COOH
OPR3
β-oxidation
OPC-8:0
COOH
COOH
4,5-ddh-JA
β-oxidation
OPR2
COOH
JAR1
NH
HO2C
JA
JA-Ile
B
Mock
MeJA
Col-0
opr2opr3
aos
Col-0
opr2opr3
aos
kDa
α-AOC
25
No Stain™
55
C
Col-0
opr2opr3
aos
AOC proteins relative intensity
Mock pretreated
MeJA pretreated
D
LOX2
AOS
AOC2
OPR3
Relative expression
Mock -Wounding
MeJA -Wounding
MeJA +Wounding
E
cis-OPDA
dn-OPDA
JA
JA-Ile
content (nmol·g-1 FW)

**Figure 1: MeJA pretreatment restitutes AOC protein levels in the mutants and OPDA content in the *opr2opr3* mutant.**

**(A)** Synthesis of jasmonic acid (JA)/JA-Ile from α-linolenic acid (α-LeA). The biosynthesis starts with the release of α-LeA from chloroplast membrane galactolipids and its conversion to (13S)-hydroperoxyoctadecatrienoic acid (13-HPOT) by 13-LIPOXYGENASE (LOX). *cis*-(+)-12-oxophytodienoic acid (*cis*-OPDA) is formed in the chloroplast (green background) from 13-HPOT through sequential actions of ALLENE OXIDE SYNTHASE (AOS) and ALLENE OXIDE CYCLASE (AOC). In the peroxisomes (yellow background) reduction of cyclopentenone ring of *cis*-OPDA is catalyzed by a peroxisomal OPDA REDUCTASE (OPR3) resulting in the formation of 3-oxo-2-(20(Z)-pentenyl)-cyclopentane-1-octanoic (OPC-8:0). Shortening of the octanoic acid side chains of OPC-8:0 by three rounds of β-oxidation yields JA. The cytosol-released JA is conjugated to Isoleucine (Ile) by the enzyme JASMONATE RESISTANT 1 (JAR1) resulting in the major bulk formation of the biologically active JA-Ile. *cis*-OPDA can directly undergo three rounds of β-oxidation yielding 4,5-didehydro-JA (4,5-ddh-JA) in a parallel OPR3-bypass pathway. The formed 4,5-ddh-JA is released to the cytosol and then reduced to JA by OPR2 and results in JA-Ile formation. Enzymes shaded in green, yellow and blue are located in the plastids, peroxisomes and cytosol, respectively.

**(B)** AOC protein content in seedlings pretreated with 1 µM MeJA or water (Mock) visualized by immunoblot, equal loading is depicted by staining with No-Stain™ Protein Labeling Reagent.

**(C)** AOC band intensity detected by immunoblot and quantified relative to total protein loading determined by Ponceau S.

**(D)** RT-qPCR of JA-responsive genes *LOX2*, *AOS*, *AOC2* and *OPR3* showing transcript accumulation at control condition (-wounding) and at 1 h after wounding with forceps. Seedlings were either pretreated with MeJA or water (Mock) during development.

**(E)** levels of *cis*-OPDA, *dn*-OPDA, JA and JA-Ile in seedlings of wild-type (Col-0), *opr2opr3*, and *aos* at control condition (-wounding) and 1 h after wounding with forceps.

Seedlings were either pretreated with MeJA or water (Mock) during development (see Supplemental Figure 2A for experimental set-up). Bars represent means of three biological replicates with 120 seedlings each (single dots) ±SEM. Statistically significant differences among genotypes within each condition were calculated using One-Way ANOVA followed by Tukey-HSD and are indicated by asterisks with *$p<0.05$, **$p<0.01$, ***$p<0.001$, and ****$p<0.0001$.

Abbreviations for compounds: 13-HPOT, (13S)-hydroperoxyoctadecatrienoic acid; cis-(+)-OPDA, *cis*-(+)-12- oxophytodienoic acid; dn-OPDA, dinor-12-oxo phytodienoic acid, OPC-8:0, 3-oxo-2-(2-pentenyl)- cyclopentane-1-octanoic acid; 4,5-ddh-JA, 4,5-didehydrojasmonic acid; JA, jasmonic acid; JA-Ile, jasmonoyl isoleucine.

Abbreviations for enzymes: LOX, lipoxygenase; AOS, allene oxide synthase; AOC, allene oxide cyclase; OPR3, 12-oxophytodienoate-10,11-reductase 3; OPR2, 12-oxophytodienoate-10,11-reductase 2; JAR1, jasmonoyl-isoleucine synthetase.

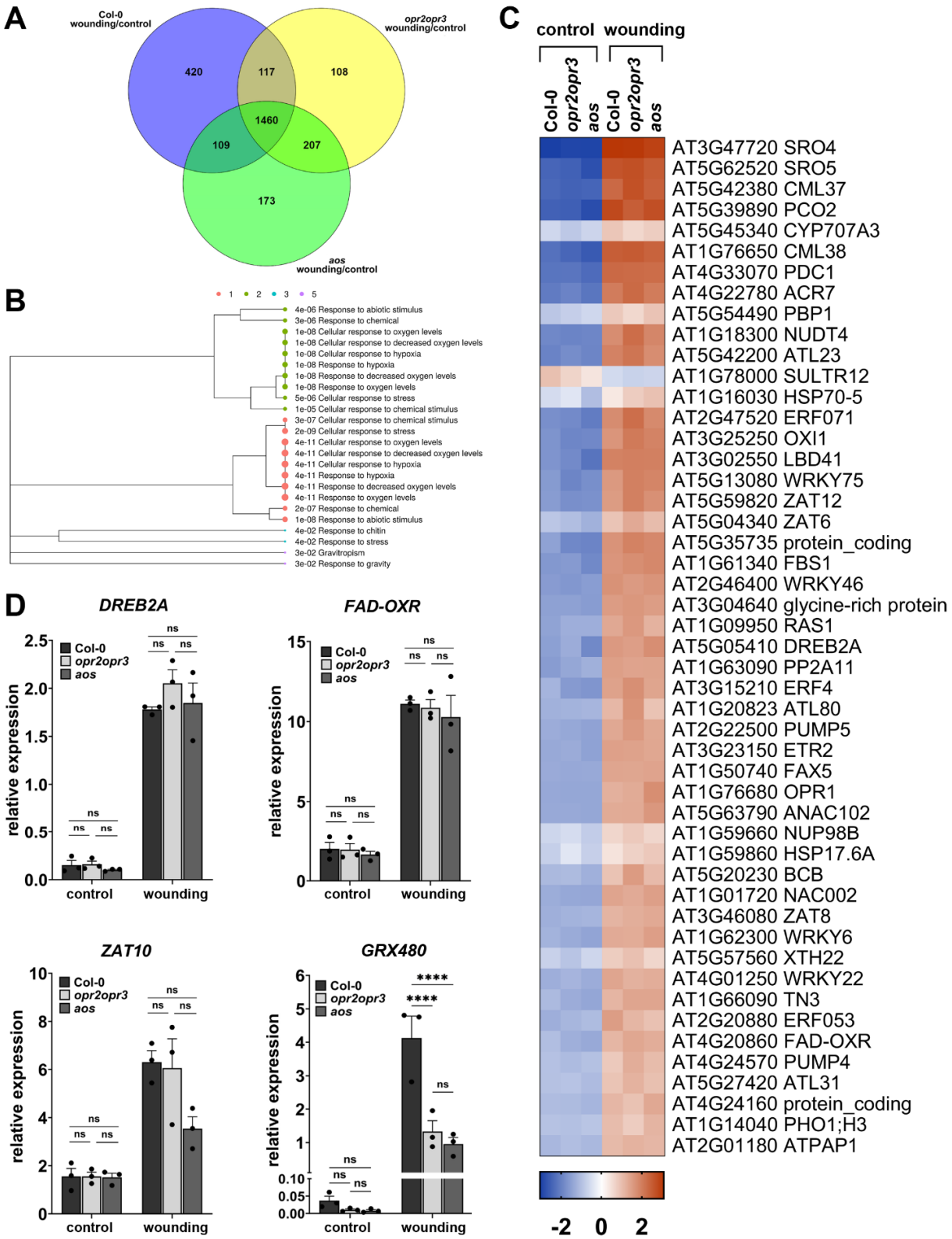
A
Col-0 wounding/control
opr2opr3 wounding/control
aos wounding/control
420
117
108
1460
109
207
173
B
1 2 3 5
4e-06 Response to abiotic stimulus
3e-06 Response to chemical
1e-08 Cellular response to oxygen levels
1e-08 Cellular response to decreased oxygen levels
1e-08 Cellular response to hypoxia
1e-08 Response to hypoxia
1e-08 Response to decreased oxygen levels
1e-08 Response to oxygen levels
5e-06 Cellular response to stress
1e-05 Cellular response to chemical stimulus
3e-07 Cellular response to chemical stimulus
2e-09 Cellular response to stress
4e-11 Cellular response to oxygen levels
4e-11 Cellular response to decreased oxygen levels
4e-11 Cellular response to hypoxia
4e-11 Response to hypoxia
4e-11 Response to decreased oxygen levels
4e-11 Response to oxygen levels
2e-07 Response to chemical
1e-08 Response to abiotic stimulus
4e-02 Response to chitin
4e-02 Response to stress
3e-02 Gravitropism
3e-02 Response to gravity
C
control wounding
Col-0 opr2opr3 aos Col-0 opr2opr3 aos
AT3G47720 SRO4
AT5G62520 SRO5
AT5G42380 CML37
AT5G39890 PCO2
AT5G45340 CYP707A3
AT1G76650 CML38
AT4G33070 PDC1
AT4G22780 ACR7
AT5G54490 PBP1
AT1G18300 NUDT4
AT5G42200 ATL23
AT1G78000 SULTR12
AT1G16030 HSP70-5
AT2G47520 ERF071
AT3G25250 OXI1
AT3G02550 LBD41
AT5G13080 WRKY75
AT5G59820 ZAT12
AT5G04340 ZAT6
AT5G35735 protein_coding
AT1G61340 FBS1
AT2G46400 WRKY46
AT3G04640 glycine-rich protein
AT1G09950 RAS1
AT5G05410 DREB2A
AT1G63090 PP2A11
AT3G15210 ERF4
AT1G20823 ATL80
AT2G22500 PUMP5
AT3G23150 ETR2
AT1G50740 FAX5
AT1G76680 OPR1
AT5G63790 ANAC102
AT1G59660 NUP98B
AT1G59860 HSP17.6A
AT5G20230 BCB
AT1G01720 NAC002
AT3G46080 ZAT8
AT1G62300 WRKY6
AT5G57560 XTH22
AT4G01250 WRKY22
AT1G66090 TN3
AT2G20880 ERF053
AT4G20860 FAD-OXR
AT4G24570 PUMP4
AT5G27420 ATL31
AT4G24160 protein_coding
AT1G14040 PHO1;H3
AT2G01180 ATPAP1
-2 0 2
D
DREB2A
FAD-OXR
ZAT10
GRX480
Col-0
opr2opr3
aos
relative expression
control
wounding
ns
****

**Figure 2: The JA/OPDA-independent wound response of seedlings.** Ten-day old seedlings from Col-0, *opr2opr3* and *aos* were pretreated with MeJA during development and were either unwounded (control) or harvested 1 h post wounding with forceps (wounding).

**(A)** Venn diagram showing the wound response in Col-0 compared to *opr2opr3* and *aos* mutants. Differentially expressed genes (DEGs) after wounding compared to non-wounded control for each genotype showed a common response with 1460 DEGs. DEGs were identified using FDR and FC cutoffs of 0.05 and 2, respectively.

**(B)** Hierarchical cluster tree summarizing significant biological pathways enriched in the 1460 DEGs common to all genotypes from (A). Gene ontology analysis was performed based on biological process.

**(C)** Heatmap illustrating 50 out of 211 DEGs enriched in the GO term 'response to stress' from **(B)**. Average FPKM values of three independent biological replicates were transformed into row normalized Z-Score.

**(D)** RT-qPCR validation of DEGs previously described as OPDA-responsive genes. Transcript accumulation of *FAD-OXR*, *DREB2A*, *ZAT10* and *GRX480* in Col-0, *opr2opr3* and *aos* at control and wounding conditions. Transcript levels were normalized to those of *PP2A*. Bars represent means of three biological replicates ±SEM. Statistically significant differences among genotypes within each condition were calculated using One-Way ANOVA followed by Tukey-HSD and are indicated by asterisks with ****$p<0.0001$; ns = non-significant.

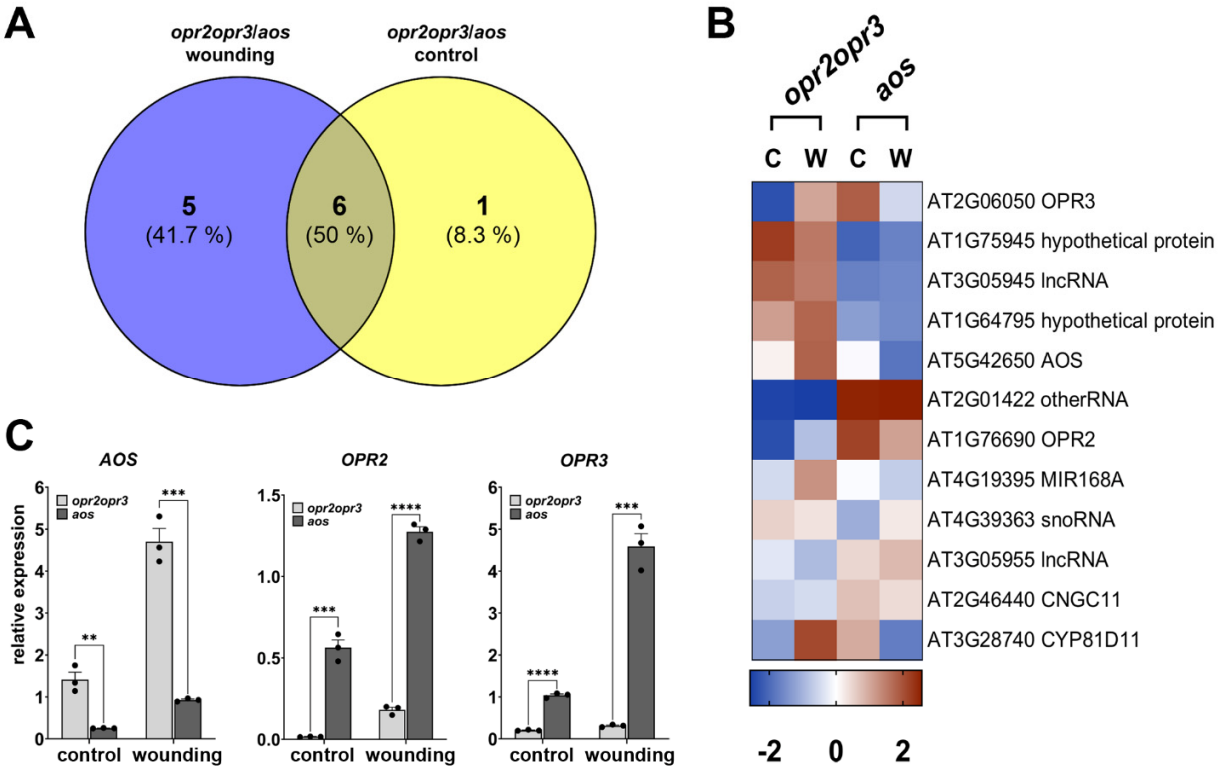


**Figure 3: The OPDA-specific transcriptional change deduced from transcriptomic comparison between seedlings of *opr2opr3* and aos at control and wounding conditions.** Ten-day old seedlings from *opr2opr3* and *aos* were pretreated with MeJA during development and were either unwounded (control, C) or harvested 1 h post wounding with forceps (wounding, W).

**(A)** Venn diagram representing genes showing differential expression when *opr2opr3* is compared to *aos* at control and wounding conditions (FDR cutoff = 0.05 and FC cutoff = 2).

**(B)** Heatmap illustrating the expression levels of the eleven wounding-related DEGs from (A). The average FPKM values of three independent biological replicates were transformed into row-normalized Z-Score.

**(C)** Transcript accumulation of *AOS*, *OPR2,* and *OPR3* selected from **(B)** and determined by RT-qPCR. Transcript levels were normalized to those of *PP2A*. Bars represent means of three biological replicates (single dots; ±SEM). Asterisks denote statistically significant differences among genotypes as determined by Student's t-test within each condition (** $p<0.01$, *** $p<0.001$, **** $p<0.0001$).

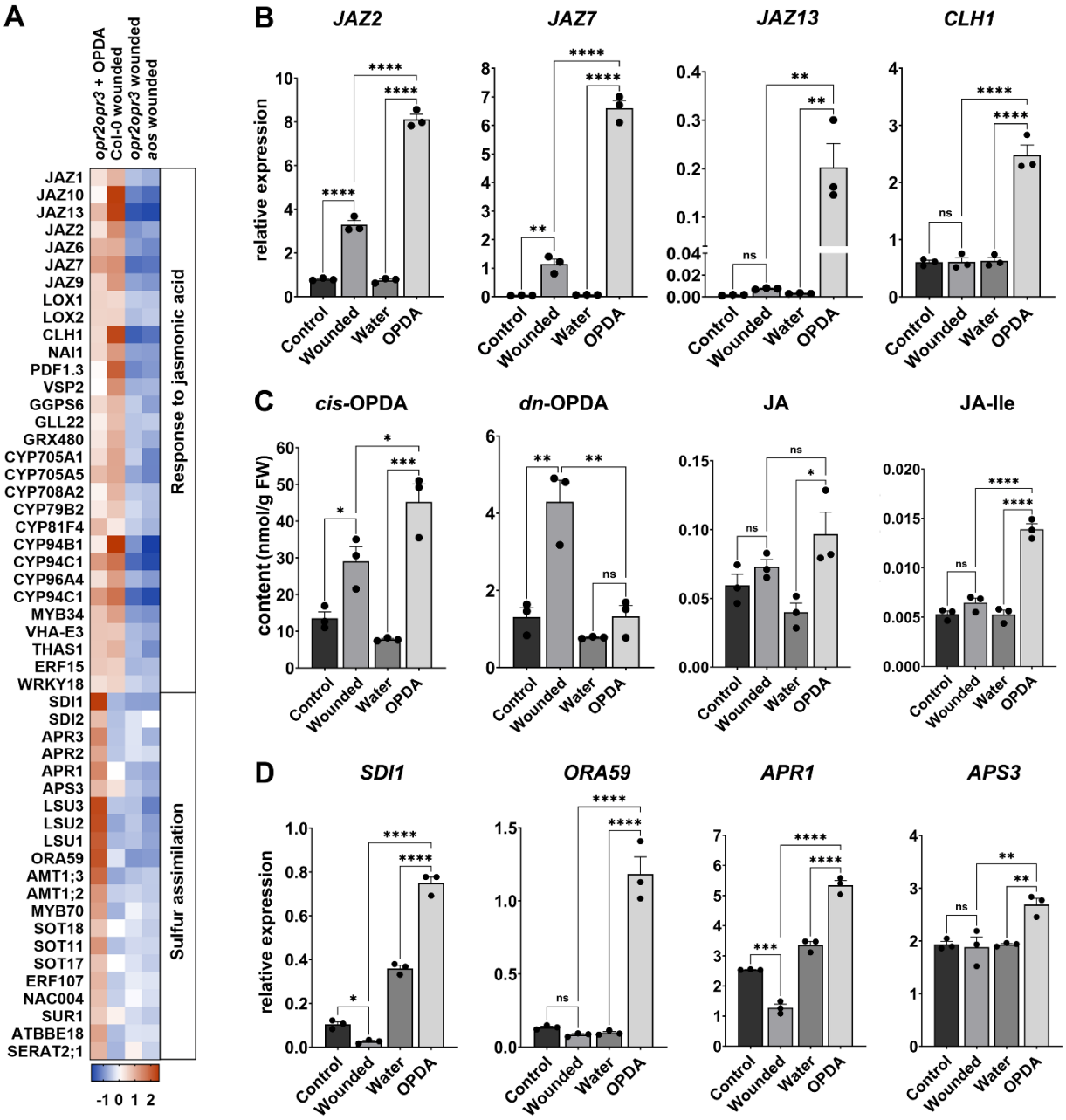


**Figure 4: Application of OPDA results in the induction of JA-Ile signaling and sulfur metabolism.**

**(A)** Heatmap of DEGs showing enrichment in JA signaling pathway genes and genes involved in sulfur assimilation in seedlings of *opr2opr3* following application of 25 µM OPDA for 30 min. DEGs were plotted and compared to those from wounded seedlings of Col-0, *opr2opr3* and *aos*

using average FPKM values transformed into row-normalized Z-score of three biological replicates.

**(B)** RT-qPCR validation of the up-regulation of JA-responsive genes *JAZ2*, *JAZ7*, *JAZ13* and *CLH1* in *opr2opr3* seedlings treated with OPDA in comparison to wounded *opr2opr3* seedlings. OPDA-treated and wounded *opr2opr3* seedlings were compared to their respective controls, non-wounded (control) and water-treated seedlings, respectively.

**(C)** *cis*-OPDA, *dn*-OPDA, JA and JA-Ile accumulation in *opr2opr3* seedlings treated with OPDA in comparison to wounded *opr2opr3* seedlings producing OPDA endogenously.

**(D)** RT-qPCR validation of the up-regulation of the sulfur metabolism genes *SDI1*, *ORA59*, *APR1* and *APS3* in *opr2opr3* seedlings treated with OPDA in comparison to wounded *opr2opr3* seedlings. OPDA-treatment and wounding of seedlings were compared to seedlings which were non-wounded (control) and water-treated (water), respectively.

Bars **(B-D)** represent means of three biological replicates with 120 seedlings each (single dots; ±SEM). Statistically significant differences among treatments were calculated using One-Way ANOVA followed by Tukey-HSD and are indicated by asterisks with *$p<0.05$, **$p<0.01$, ***$p<0.001$, and ****$p<0.0001$; ns = non-significant.

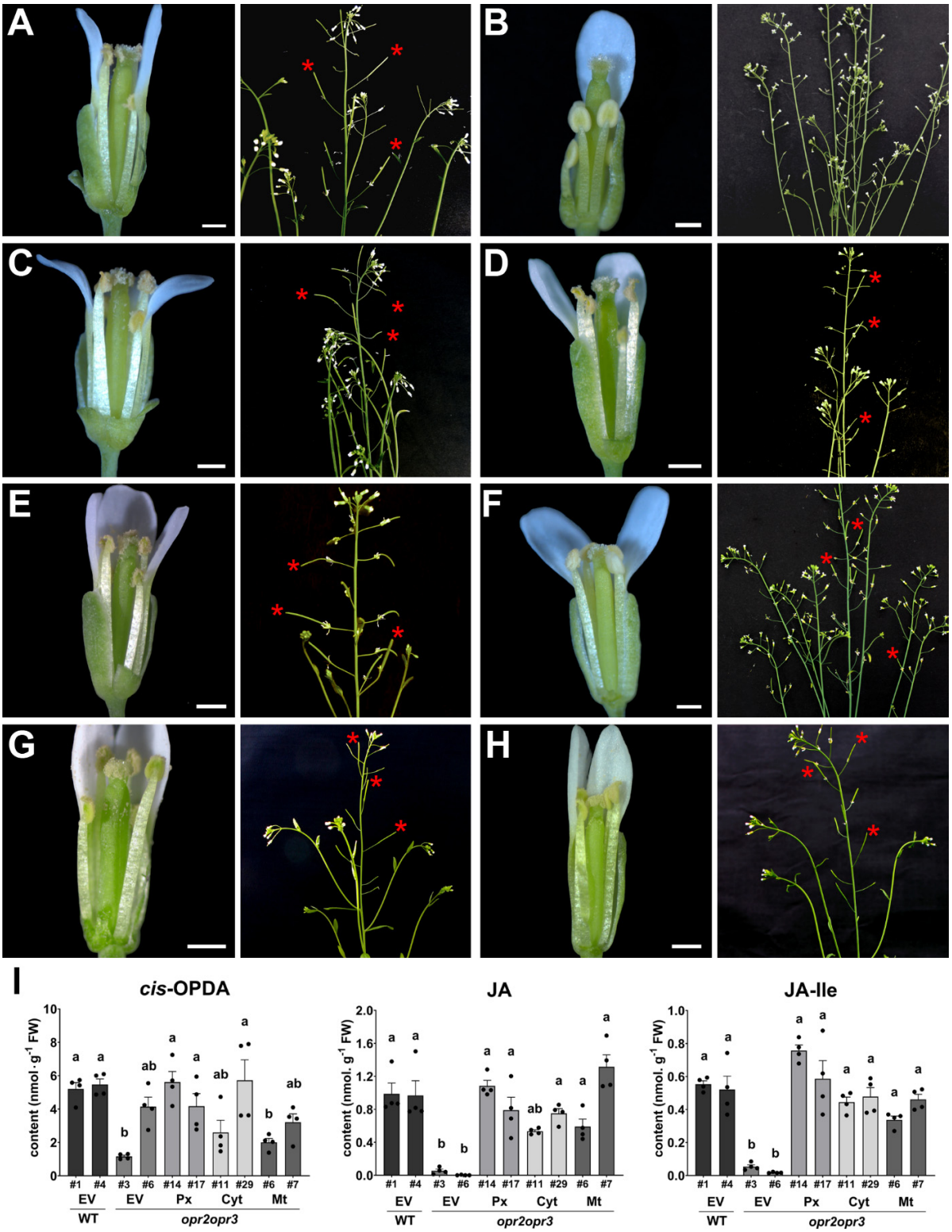
A
B
C
D
E
F
G
H
I
cis-OPDA
JA
JA-Ile
content (nmol·g-1 FW)
content (nmol. g-1 FW)
#1 #4 #3 #6 #14 #17 #11 #29 #6 #7
EV
WT
EV
Px
Cyt
Mt
opr2opr3

**Figure 5: Restitution of the fertility and JA/JA-Ile levels of *opr2opr3* plants by OPR3-targeted to different organelles.**

**(A-H)** Open flower buds showing stamen filament elongation and pollen release by anthers (scale bars represent 0.5 mm) and plant inflorescences showing silique formation at days 50-60 post germination with asterisks marking fully developed siliques. Col-0 and *opr2opr3* transformed with an empty vector **(A, B)** show fertility and sterility, respectively. *opr2opr3* T2 lines complemented with peroxisome- **(C)**, nucleus- **(D)**, cytosol- **(E)**, ER- **(F)**, plastid stroma- **(G)** and mitochondria- **(H)** targeted OPR3 fused to YFP show the rescue of the *opr2opr3* sterility phenotype.

**(I)** *cis*-OPDA, JA and JA-Ile accumulation at 1 h after wounding of seedlings of wild type (WT) or *opr2opr3* transformed with either empty vector (EV) or *35S::OPR3* targeted to peroxisomes (Px), cytosol (Cyt) or mitochondria (Mt). Numbers refer to independent transgenic lines, which were selected for single insertion and homozygosity. Bars represent means of four biological replicates with 120 seedlings each (single dots; ±SEM). Statistically significant differences between *opr2opr3* transformed with empty vector and transformed with the OPR3 constructs were calculated using One-Way ANOVA followed by Tukey HSD ($p<0.05$) and are denoted by different letters.

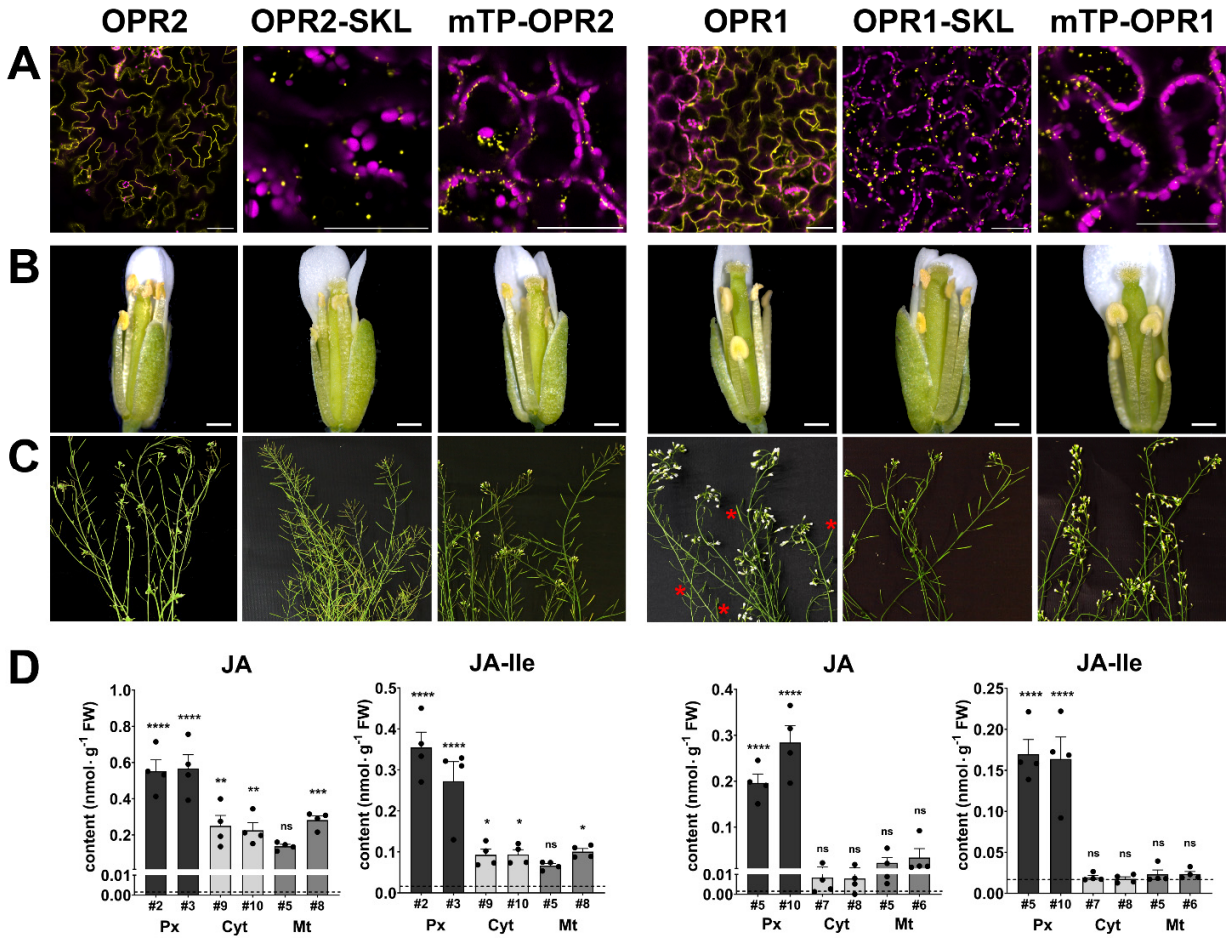


**Figure 6: Restitution of the fertility and JA/JA-Ile levels of *opr2opr3* plants by OPR2, but not by OPR1, both targeted to different organelles.**

Stable *opr2opr3* complementation lines expressing OPR2 (left) or OPR1 (right) targeted to the cytosol (without any signal peptide), to the peroxisomes (OPR-SKL) or to mitochondria (mTP-OPR), all under control of the CaMV *35S* promoter.

**(A)** Micrographs showing the correct localization of the respective OPR-YFP-fusion. The yellow signal corresponds to OPR-YFP, whereas the magenta signal corresponds to chlorophyll autofluorescence. Scale bars represent 50 µm.

**(B, C)** Open flower buds to show stamen filament elongation and pollen release by anthers **(B)** and plant inflorescences showing silique formation at days 50-60 post germination **(C)**. Note that transformation of *opr2opr3* with all variants of OPR2 and with OPR1 targeted to peroxisomes resulted in a rescue of fertility visible by elongated filaments and fully developed siliques. Targeting of OPR1 to cytosol led to partial rescue shown by few fully developed siliques only (red

asterisks), whereas targeting of OPR1 to mitochondria did not rescue fertility. Scale bars in **(B)** represent 0.5 mm.

**(D)** JA and JA-Ile accumulation at 1 h after wounding of seedlings of *opr2opr3* transformed with either *35S::OPR2* or *35S::OPR1*, either targeted to cytosol (Cyt), peroxisomes (Px), or mitochondria (Mt). Numbers refer to independent transgenic lines, which were selected for single insertion and homozygosity. The mean levels of JA/JA-Ile of *opr2opr3* are taken from Figure 7 and are represented by dashed lines for comparison. Bars represent means of four biological replicates with 120 seedlings each (single dots; ±SEM). Statistically significant differences between *opr2opr3* transformed with the different *OPR2* and *OPR1* constructs and *opr2opr3* were calculated using One-Way ANOVA with Fisher LSD post-hoc test and are indicated by asterisks with *$p<0.05$, **$p<0.01$, ***$p<0.001$, and ****$p<0.0001$; ns = non-significant.

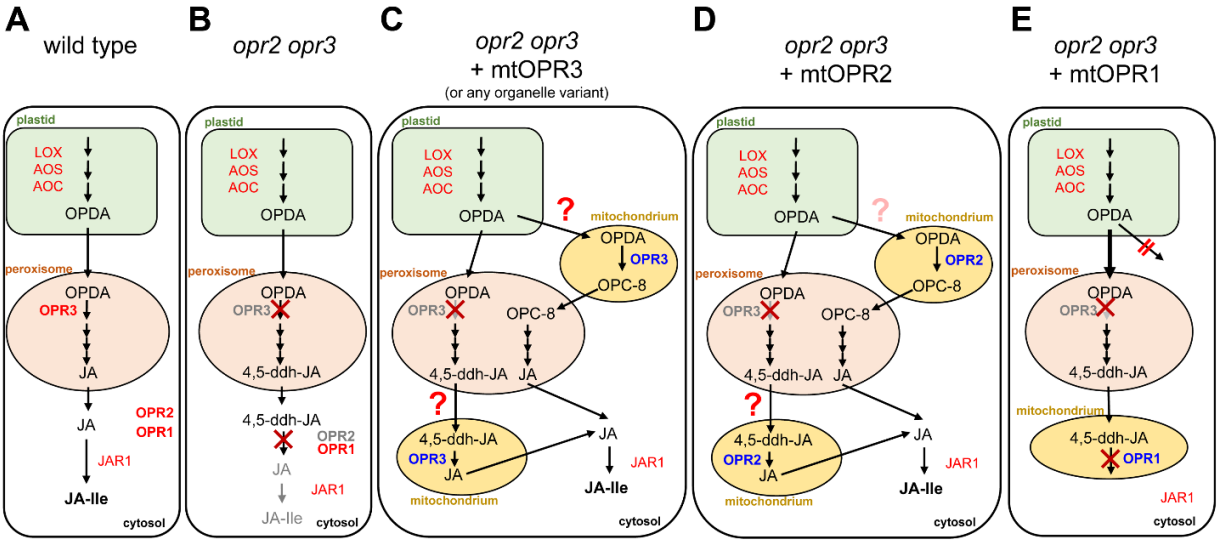


**Figure 7: Schematic picture on the approaches leading to insights about the putative distribution of OPDA and 4,5-ddh-JA within cells of a wounded Arabidopsis seedling.**

Putative subcellular distribution of OPDA and its conversion to JA deduced from the trans-organellar complementation approach.

**(A)** In wild-type plants, OPDA is converted to JA in the peroxisome through the OPR3 canonical route, the contribution of OPR2 located in the cytosol appears to be neglectable but comes into place if OPR3 is not functional (e.g., *opr3* single mutant, Chini et al., 2018).

**(B)** The interruption of both routes in the *opr2opr3* mutant results in conversion of OPDA to 4,5-ddh-JA which is not metabolized to JA/JA-Ile.

**(C)** Targeting of OPR3 to any organelle in *opr2opr3* mutant plants (depicted for mitochondrial localization) restitutes JA biosynthesis in this mutant. If this is a result of either an ability of OPDA or of its β-oxidation product, 4,5-ddh-JA, to translocate to other cell compartments cannot be decided by this approach, since OPR3 is active to convert OPDA and 4,5-ddh-JA (red question marks). Trans-organellar complementation by using OPR2 or OPR1 targeted into mitochondria, however, helped to clarify this point.

**(D)** Mitochondrial targeting of OPR2 with its specificity to 4,5-ddh-JA complemented JA biosynthesis favoring rather an ability of 4,5-ddh-JA to be mobile, although the conversion of OPDA can still not be excluded due to some activity of OPR2 towards OPDA (light red question mark).

**(E)** As final proof, OPR1 was targeted to mitochondria, because OPR1 is specific for OPDA and does not convert 4,5-ddh-JA. Expression of mtOPR1 in *opr2opr3* did not restitute JA/JA-Ile production. Even the very limited JA formation by cytosolic OPR1 suggests restricted occurrence of OPDA in this compartment (not shown in this scheme, data see Figure 6). The lack of JA formation by mitochondrial OPR1 and the diminished JA formation by cytosolic OPR1 suggest that OPDA may not have the ability to access these cellular compartments and might strongly compartmentalized in the organelles involved in JA biosynthesis, the plastids and peroxisomes.